Electrochimica Acta 435 (2022) 141389

Contents lists available at ScienceDirect

Electrochimica Acta

journal homepage: www.journals.elsevier.com/electrochimica-acta

The phenomenon of increasing capacitance induced by 1T/2H-MoS_2 surface modification with Pt particles – Influence on composition and energy storage mechanism

Zuzanna Zarach [a,*], Mariusz Szkoda [a,b], Konrad Trzciński [a,b], Marcin Łapiński [b,c], Grzegorz Trykowski [d], Andrzej P. Nowak [a,b]

[a] Department of Chemistry and Technology of Functional Materials, Faculty of Chemistry, Gdańsk University of Technology, Gabriela Narutowicza 11/12, 80-233 Gdańsk, Poland
[b] Advanced Materials Center, Gdańsk University of Technology, Gabriela Narutowicza 11/12, 80-233 Gdańsk, Poland
[c] Institute of Nanotechnology and Materials Engineering, Faculty of Applied Physics and Mathematics, Gdańsk University of Technology, Narutowicza 11/12, 80-233 Gdańsk, Poland
[d] Faculty of Chemistry, Nicolaus Copernicus University in Toruń, Gagarina 7, 87-100, Toruń, Poland

ARTICLE INFO

Keywords:
Molybdenum disulfide
Non-stochiometric molybdenum oxides
Platinum dissolution-deposition
Supercapacitors
Energy storage

In this paper, several approaches to the synthesis of molybdenum-based electrode materials for supercapacitors are presented, including anodization, hydrothermal process and annealing. For the material prepared via anodization of a molybdenum plate, followed by a hydrothermal process in thiourea aqueous solution, a thorough study of the Pt-surface modification through repetitive cycling in 1 M sulfuric acid with Pt acting as a counter electrode is performed, including X-ray photoelectron spectroscopy analysis and energy storage mechanism contribution. Along with the increasing number of cycles, an increase of the capacitance value is observed up to 1.064 F cm^{-2} after 60 000 cycles, resulting in more than tenfold growth (by over 1 150%). The analysis reveals progressive changes in the electrode material's chemical composition and the increasing pseudocapacitance contribution in energy storage processes, which is strictly caused by the formation of mixed molybdenum oxides with oxygen vacancies. Thus, Pt-surface modification effectively improves the electrochemical performance of the electrode material with excellent coulombic efficiency and capacitance retention. In a symmetric two-electrode configuration with Pt-modified electrode materials, the areal capacitance of 140.5 mF cm^{-2} is obtained after 50 000 cycles (with capacitance retention of 123%) indicating that Pt-surface modification of MoS_2 may provide a novel approach for electrode materials for high-performance supercapacitors.

1. Introduction

Nowadays, the whole world is struggling with environmental problems related to the pollution caused by the use of fossil fuels. These problems do not end with pollution, as it is known that the depletion of these sources could soon lead to an energy crisis. As a consequence, a majority of countries have currently been focusing on the use of renewable energy sources, which can be a solution to this emerging problem. However, it is important to be aware of the limitation of their periodic availability, which is especially noticeable in the case of solar or wind energy. The answer to this problem may be the application of effective and efficient technologies that will enable the storage of energy in order to use it at the most convenient time. Supercapacitors, also known as electrochemical capacitors, are one of energy storage systems that exhibit higher energy density than conventional capacitors and higher power density than batteries[1,2].

What is more, in energy storage devices such as batteries or supercapacitors, binders are quite often an inherent element, which does not support the energy storage process, but plays role in improving physical contacts. However, their use also contributes to the deterioration of some parameters of the device, causing the reduction of volumetric and gravimetric capacitance. Its presence also may contribute to the occurrence of side reactions during the charging and discharging processes, usually leading to additional costs, and in the case of the binders such as polyvinylidene fluoride, an additional increase in the resistance value may be observed[3,4]. Therefore, the synthesis of the electrode material directly on the current collector is an eminently desirable process in obtaining the superior overall performance of the energy storage device.

* Corresponding author.
E-mail address: zuzanna.zarach@pg.edu.pl (Z. Zarach).

https://doi.org/10.1016/j.electacta.2022.141389
Received 25 August 2022; Received in revised form 14 October 2022; Accepted 16 October 2022
Available online 20 October 2022

Transition metal dichalcogenides, in particular, are gaining more and more attention in terms of their use as energy storage electrode materials, precisely because of their layered structure and the weak van der Waals bonds between the individual layers [5,6], which enable fast charging and discharging, while maintaining stability comparable to that offered by two-dimensional carbon materials [7–9]. MoS_2 structure consists of three planes in the order of S-Mo-S, with molybdenum sandwiched between two sulfur layers[10] (see Fig. 2**a,b**). Depending on which phase of MoS_2 is investigated, it is characterized by distinctive features. When it comes to energy storage applications, the most attention is paid to the 1T trigonal and the 2H hexagonal MoS_2 structure. Octahedral 1T phase is a metallic one, which is mainly obtained through the transition from the 2H phase by an electron beam application, laser irradiation, or ion intercalation process [11–13]. Obtaining a 1T phase is particularly desirable and the research is directed toward this one mainly due to its high conductivity, although its stability is still a challenge to face. On the contrary, the 2H phase, which is a trigonal prismatic structure, possesses semiconductive properties and exceeds other polymorphs in terms of stability. Sakar et al. reported molybdenum sulfide electrode material, containing both 1T and 2H phases, that exhibited a volumetric capacitance of 212 F cm^{-3} and even 343 F cm^{-3} when it was combined with reduced graphene oxide [14]. Furthermore, a thin film of MoS_2 obtained by Pujari et al. using low temperature soft chemical synthesis approach was characterized by the volumetric capacitance of 911 F cm^{-3} [15]. MoS_2 synthesis through DC sputtering was also shown to be an effective way to obtain thin, nanostructured films of specific capacitance of 138 F g^{-1} and the cycling ability of 86% after 5 000 cycles [16]. In another report by Acerce et al.[17], metallic 1T MoS_2 phase exhibited the volumetric capacitance ranging from 400 to 700 F cm^{-3}, depending on the aqueous electrolyte that had been used.

When characterizing electrode materials for energy storage, a commonly used counter electrode is platinum, also for materials with other applications, such as electrochemical hydrogen evolution reaction (HER), photoelectrochemical water splitting and amperometric sensors. It is well known that, due to its excellent electrochemical inertness, electrical conductivity and mechanical stability, platinum is considered to be one of the most appropriate materials for use as a counter electrode in electrochemical measurements. However, Cervino et al. were the first to describe that platinum may undergo dissolution at high anodic potentials in an acidic environment [18]. The influence of polarization on the dissolution was also observed by some other authors, as well [19–21]. Apart from that, there are other several factors that may affect the rate of Pt dissolution like temperature, scan rate, and potential range [22–26]. Moreover, some recent reports on the use of a Pt electrode in HER measurements also indicate that the Pt electrode may undergo an electrochemical dissolution-deposition process and thus greatly affect the experimental results [19,27–29]. As a matter of fact, the phenomenon of platinum dissolution has already been widely studied in relation to fuel cells application, and recently the issue has also been raised by Wei et al. questioning its use as a counter electrode in HER measurements [30], but it was also pointed by Jerkiewicz [31] that a great deal of the knowledge regarding platinum electrochemistry is undocumented. Furthermore, many reports not only on MoS_2, but also other transition-metal dichalcogenides, as well as carbon materials indicate that the dissolution-deposition phenomenon of Pt but also the doping itself can be used to improve the properties of an electrode material [20,21,32–36]. However, most reports on this topic primarily deal with hydrogen evolution reactions and thus, we believe that this is the first time when the phenomena is observed in the electrochemical measurements performed for electrode materials with application for energy storage in supercapacitors.

Furthermore, there are no reports about a change in the chemical composition of the material upon Pt doping and/or repetitive cycling. In the literature, MoS_2 conversion to MoO_3 was reported by Ko et al.[37]. using plasma oxidation. The transformation was also obtained by ambient pressure X-ray photoelectron spectroscopy combined with heat treatment [38]. Recently Hou et al. investigated the phase transition of MoS_2 during sodiation in charge/discharge cycles, indicating that one of the intermediate products is metallic Mo, some of which oxidizes during the charging process, resulting in MoO_3 and oxygen-deficient MoO_x [39]. The presence of molybdenum oxides in electrode materials for energy storage has been extensively considered due to their promising specific capacitance, multiple oxidation states, and environmental friendliness. Especially when it comes to molybdenum oxides with intrinsic oxygen vacancies, they are highly attractive as they are characterized by greatly increased conductivity [40,41] but which was also presented by Dunn et al., oxygen vacancies facilitate faster charge storage kinetics, leading to improved capacitance and cycle life [40]. Furthermore, it is often recognized that molybdenum-based oxides have limited cycle life and poor performance hinders the application for long-term energy storage applications. To increase capacitance retention, several approaches are being introduced. As an example, Cai et al. stated that by introducing K^+ into the MoO_x structure, it was possible to shift from Mo^{5+}/Mo^{6+} to Mo^{4+}/Mo^{5+} charge storage redox couple. As a consequence, both the conductivity and the overall electrochemical performance were enhanced, altogether with the prolonged cycle life of the supercapacitor [42].

In most of the cases observed with MoS_2-based materials for energy storage applications, the material degrades after repeated charging and discharging cycles, resulting in a decreasing capacitance. The phenomenon of capacitance increase was observed in several literature reports, however, it was temporary and only observed in the initial charge and discharge cycles [43], as generally for MoS_2-based electrode materials it is typical to observe a gradual degradation of specific capacitance with subsequent cycles, which is a major limitation in long-term energy storage applications. The exception is the work presented by Bissett et al., who reported a significant increase in capacitance during the first 3 000 cycles for MoS_2/graphene composite, which was attributed to the progressive exfoliation of the material, associated with ion intercalation/deintercalation [44]. Furthermore, little work has so far analyzed what happens to the material during charge/discharge cycles. Several reports only indicate phase transition occurring during the intercalation and deintercalation of lithium or sodium ions in the materials used in battery applications, including MoS_2-based materials [45–48]. Nonetheless, no detailed investigation of the changes taking place in the material during charge/discharge cycles was performed together with the analysis of the charge storage mechanism, with the simultaneous observation of the phenomenon of a significant increase in specific capacitance.

Therefore, in this work, several approaches to the synthesis of molybdenum-based electrode materials for supercapacitors are shown, including anodization, hydrothermal process, and annealing. Furthermore, we present a complex analysis of the Pt-surface modification during multiple charging and discharging cycles of the electrode material prepared via anodization of a molybdenum plate, followed by a hydrothermal process in thiourea aqueous solution with the energy storage mechanism study. The influence of platinum-surface modification and using platinum as a counter electrode on charge storage performance and charge storage mechanism in studied electrode material is investigated as well. It was shown that the prolonged process of modification of the electrode surface with platinum enhanced the phenomenon of the capacitance increase. After 60 000 cycles, the specific capacitance of the electrode material modified with Pt particles increased to over 1 F cm^{-2}, whereas the symmetric two-electrode system reached a capacitance of 140 mF cm^{-2} and in each case, the coulombic efficiency was above 97% during all the cycles. Furthermore, this study reveals the changes taking place in the composition of the molybdenum disulfide thin layer, presenting the transition to mixed molybdenum oxides. Together with the transition from sulfides to oxides and introduction of oxygen vacancies, the contribution of the pseudocapacitive energy storage mechanism is enhanced. It is also emphasized that when Pt counter electrode is used in the study of energy storage materials,

careful consideration should be given to the investigation due to the dissolution-deposition phenomenon of platinum.

2. Experimental section

Chemicals used: Molybdenum (Mo) foil (0.05 mm thick, 99.95%) (Alfa Aesar) was sonicated in acetone (C_3H_6O) and isopropanol (C_3H_8O) (both obtained from Chempur). The electrolyte for the electrochemical oxidation of titanium foil consisted of ammonium fluoride (NH_4F) p.a., ethylene glycol ($C_2H_6O_2$), phosphoric acid (H_3PO_4), all from Chempur, and distilled water. Thiourea (CH_4N_2S) used in the hydrothermal method and potassium sulfate (K_2SO_4) was purchased from Alfa Aesar and sulfuric acid (H_2SO_4) (p.a. 95%) used for electrochemical characterization was received from POCH.

Anodization of Mo foil: At first, molybdenum foil was cut into pieces, cleaned using ultrasonic treatment in isopropanol:acetone mixture (1:1 v/v) for 10 min, and eventually rinsed with distilled water. In the anodization process, the as-prepared Mo foil constituted an anode and the titanium plate was a cathode. The synthesis was carried out at a constant temperature (23 °C) using a cooling bath thermostat (KISS K6, Huber) with a voltage of 5 V applied for 2 h and the electrolyte was prepared according to the previous report [49].

Hydrothermal synthesis: The final step of electrode preparation was to perform a hydrothermal procedure. For this, an anodized molybdenum plate was placed in a Teflon-lined stainless-steel autoclave (50 mL) with thiourea (1 M) aqueous solution (25 mL). The autoclave was transferred to an oven for 24 h at 200 °C. After that, the autoclave was cooled to room temperature and the obtained plate with deposited molybdenum-based material was washed a few times with ultrapure water.

Different approaches for Mo foil modification: Apart from the electrode material that was obtained as described above, some different approaches of molybdenum foil modification were included, namely, anodic oxidation (A), hydrothermal process (H) and annealing (A450) of modified molybdenum plate were combined in different order and combination, which is accurately presented in Fig. S1. The samples were designated by the letters ascribed to the individual processes in the order in which they were carried out (e.g. Mo(AH) denotes to anodization followed by the hydrothermal process). The annealing process was performed in a tube furnace in an air atmosphere with a heating rate of 2 °C/min for over 3 h and 45 min to 450 °C and eventually hold at this temperature for 2 h.

Electrochemical Pt-surface modification: Electrochemical modification of the surface with platinum particles was carried out in a three-electrode system. The working electrode was a chosen Mo-based material and the Pt electrode was used as a counter electrode. Pt (99.9%) was in the form of a 1 cm x 1 cm mesh with a wire diameter of 0.04 mm and with a nominal aperture 0.12 mm. The modification was based on repetitive cycling in 1 M H_2SO_4 in the potential range from –0.35 V to +0.2 V vs. Ag/AgCl (3 M KCl). Up to 60 000 cycles were carried out to investigate the changes taking place in the structure of the electrode material. For comparative purposes, the material that was not modified with platinum particles was tested in a system in which the working electrode was separated from the counted electrode using an electrolytic key filled with gel electrolyte, which was 0.5 M K_2SO_4 with the addition of gelatin.

Materials Characterization: The morphology of the as prepared materials was investigated using Scanning Electron Microscopy (SEM) (FEI, Quanta 3D FEG) and Transmission Electron Microscopy (TEM) (FEI, Tecnai F20X-Twin). Element identification was performed by energy dispersive X-ray spectrometer (EDS) with energy resolution of 134 eV (EDAX, model RTEM SN9755+). SEM samples were tested directly on the synthesized molybdenum foil without preparation. Samples for TEM, after peeling off the layer from the molybdenum foil, was placed on a copper TEM grid covered with a carbon layer (Lacey type Cu 400 mesh, Plano). Measurement parameters: SEM - voltage 10–20 kV from FEG, Everhart-Thornley detector (ETD), vacuum in the chamber 10^{-4} Pa; TEM – voltage 200 kV from FEG, imaging in bright field (BF) with CCD camera (Gatan, Orius), vacuum in the chamber 10^{-4} Pa. Moreover, materials were characterized using X-ray Photoelectron Spectroscopy (Escalab 250Xi, Thermo Fisher Scientific) with Al Kα radiation and the spectra were analyzed and deconvoluted by an envelope of a Gaussian-Lorentzian sum function using the spectrometer software Avantage (Version 5.973). The vibrational characteristics of the samples were studied using micro-Raman spectrometer (Renishaw InVia) with argon laser emitting at the wavelength of 514 nm and operated at 1% of its total power (50 mW). The determination of crystal structure was performed using a diffractometer (Xpert PRO-MPD) with Cu Kα emission (λ = 0.15406 nm).

Electrochemical measurements: At first, they were performed using potentiostat/galvanostat (BioLogic VSP 2078) in three-electrode configuration. The measurements were performed in 1 M H_2SO_4 with the as synthesized electrode materials constituted as a working electrode and Pt mesh and Ag/AgCl (3 M KCl) were used as counter and reference electrode, respectively. Measurements were conducted in 1 M H_2SO_4 aqueous solution, which was used as an electrolyte for a supercapacitor's construction, too. Moreover, electrochemical impedance spectroscopy (EIS) was performed in a frequency range between 20 kHz and 100 mHz with the voltage amplitude of 10 mV. For the chosen material's characterization, various techniques have been applied, e.g. galvanostatic charge-discharge tests (GCD) with current densities ranging from 4.5 to 34 mA cm^{-2}, and cyclic voltammetry at 50 mV s^{-1} in order to determine the potential range within which an electrode material is capable of charge storage.

3. Results and discussion

3.1. Characterization of the electrode materials resulted from different Mo foil modifications

Fig. 1 presents images of molybdenum foil before (Fig. 1**a-b**) and after different modifications, obtained using Scanning Electron Microscopy. In comparison with non-modified molybdenum foil, different morphologies might be observed. In the images obtained at lower magnifications, the initial structure of the molybdenum foil, which is caused by the metal processing, can be observed. Moreover, the anodic oxidation process caused the formation of a rough and rippled surface structure (Fig. 1**c-d**). The pattern is also clearly visible for the electrodes for which anodization was the first stage of the modification. On the other hand, when Mo foil was subjected to a hydrothermal process, the film that was formed almost uniformly covered the entire surface, and the formation of moss-like nanostructures was observed (Fig. 1**c-d**). The moss-like covering of the surface is also visible for samples Mo(AH) (Fig. 1**e-f**) and Mo(AA450H) (Fig. 1**k-l**). Furthermore, when the annealing process was performed as the last stage, the formation of crystal structure in the form of cuboids and cubes is distinguished (Fig. 1**i-j**).

X-ray Photoelectron Spectroscopy measurements were also performed for the prepared samples (see Fig. 2**c-l**). For the anodized sample (Fig. 2**c and** 2**h**) spectra show that the material consists of molybdenum oxides of various oxidation states, which is quite common for the anodized molybdenum foils reported in the literature [50,51]. A confirmation may be the signal distinguished in the O1s spectrum at about 530.5 eV, which proves the presence of Mo-O bonds in the sample [52,53]. O1s spectrum reveals the presence of both hydroxide and water in the sample [54–56], which is also observed for the molybdenum foil after anodization and annealing (see Fig. 2**f and** 2**k**). The difference between both samples results from the uniformity of the molybdenum oxidation state, namely an almost complete transition to the 6+ oxidation state is observed after annealing. Recorded signals of Mo $3d_{5/2}$ and $3d_{3/2}$ at around 233 eV and 233.1 eV may be assigned to the presence of MoO_3 [57,58], which was also confirmed by Raman spectroscopy. For the remaining samples, the synthesis of which took into account the

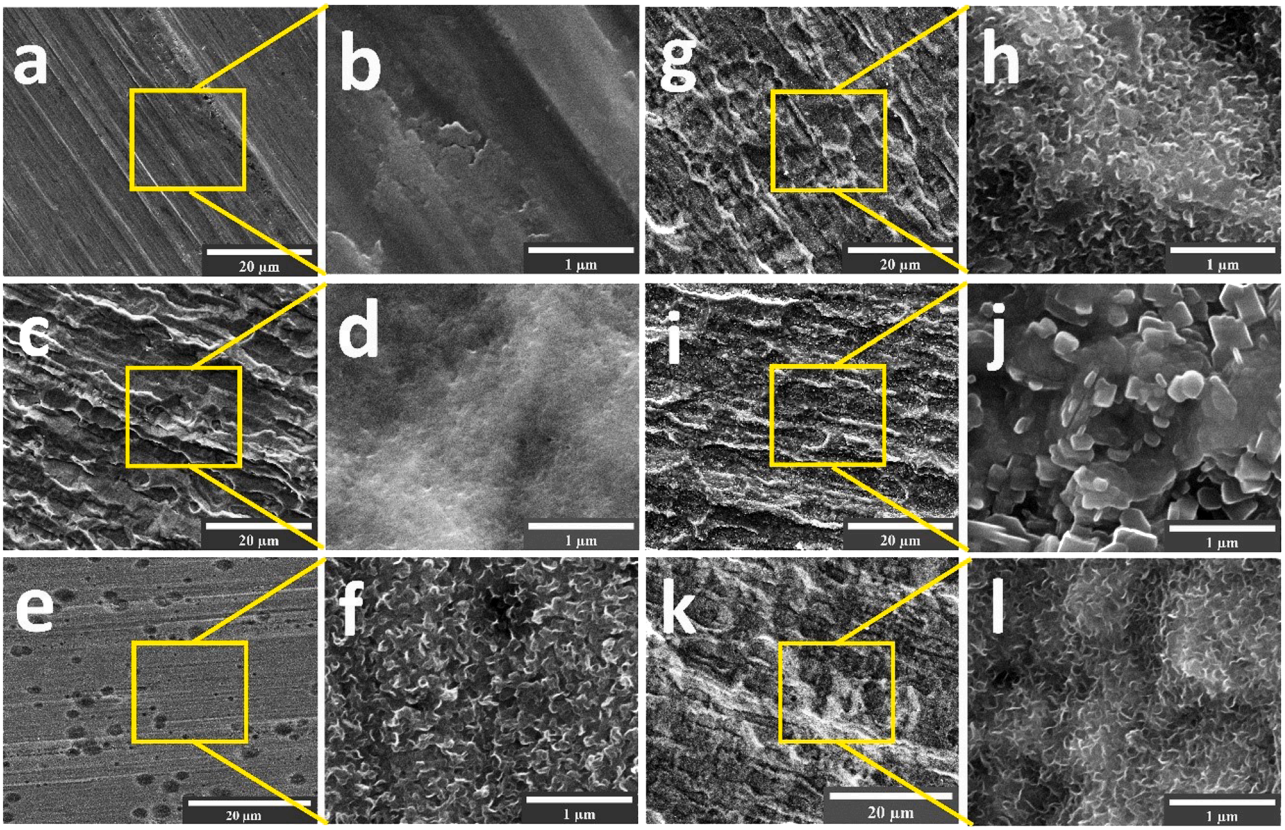

Fig. 1. SEM images for Mo foil before modifications (a-b) and after anodization Mo(A) (c-d), hydrothermal process Mo(H) (e-f), anodization and hydrothermal processes Mo(AH) (g-h), anodization and annealing Mo(AA450) (i-j) and subsequent anodization, annealing and hydrothermal processes Mo(AA450H) (k-l).

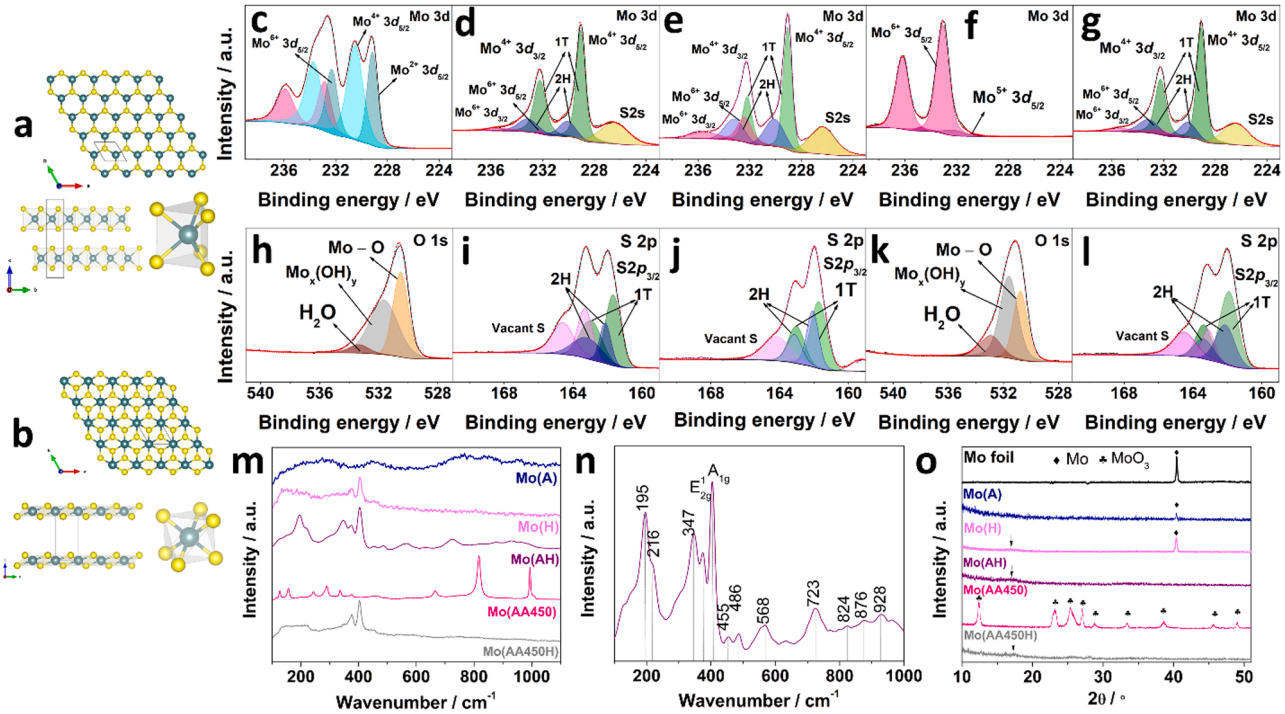

Fig. 2. Top and side views of a) 2H and b) 1T structures of the MoS_2 and the presentation of the trigonal prismatic coordination in 2H-MoS_2 and the octahedral coordination in 1T-MoS_2 for the molybdenum atom (cyan). Crystal structures created with VESTA 3 software[69]. XPS spectra of Mo foil after different modifications: Mo(A) (c,h); Mo(H) (d,i); Mo(AH) (e,j); Mo(AA450) (f,k); Mo(AA450H) (g,l); m) Raman spectra of Mo foil after different modifications with detailed spectrum (n) for the electrode material Mo(A) and Mo(AH); o) XRD spectra of Mo foil after different modifications with the magnification of the area between 10 and 50°.

hydrothermal process, the results clearly indicate that each of them contains mainly MoS_2. This is confirmed by the results presented in the Mo 3d spectra of Mo(H), Mo(AH) and Mo(AA450H) samples (see Fig. 2**d, e, g**), where two peaks at around 232.2 and 229.0 eV are related to the 1T MoS_2 phase, whereas the signals at 233.2 and 230.1 eV confirm the presence of 2H phase [14,59]. Worth noting is that the shift of 1T phase is about 1 eV from the 2H phase, which is consistent with the literature reports in each case [14,60]. At the same time, the S $2p_{1/2}$ and $2p_{3/2}$ signals (Fig. 2**i, j, l**) from 1T and 2H phases are located at 163.0 and 161.7 eV, and 163.2 and 162.1 eV, respectively [59,61]. Furthermore, the peaks located in the higher binding energy the S 2*p* spectrum may correspond to the vacant S atoms in both 1T and 2H phases [62,63]. The results also show the signals coming from molybdenum in its oxidized form (Mo^{6+}), which is present in small amounts in the form of molybdenum oxide [58,61].

The as-modified molybdenum-based electrode materials were also characterized using Raman spectroscopy. As it is shown in the Raman spectrum in Fig. 2**m**, Mo after anodization (A) is rather amorphous. When molybdenum foil was subjected to both anodization and hydrothermal process (AH), a significant amount of distinct signals can be observed in the Raman spectrum. The two most characteristic peaks at 375 cm^{-1} and 404 cm^{-1} can be attributed to the vibrations in thermostable 2H-MoS_2 molecules, which are ascribed to E^1_{2g} in-plane and A_{1g} out-plane active modes, respectively [14,59,62,64]. Those signals are also observed for the sample Mo(H), indicating the presence of 2H-MoS_2, as well. Apart from those two prominent signals, some additional peaks at spectrum of Mo(AH) could be distinguished at 195, 216 and 347 cm^{-1} that indicate the presence of the trigonal phase of MoS_2 in the analyzed sample [14,64–66]. Moreover, weak Raman modes in the range from 445 to 930 cm^{-1} may suggest that the material contains a minor amount MoO_x molecules in the intermediate oxidation state, where $2 < x < 3$ [67]. In order to present the Raman bands of Mo(AH) more clearly, this spectrum has also been presented in a separate figure (Fig. 2**n**). After modification in the form of anodization with annealing (AA450), a crystalline MoO_3 was obtained, which was confirmed by the presence of the main band at about 820 cm^{-1}, attributed to the stretching vibrations in Mo-O-Mo [57]. Another characteristic peak at 996 cm^{-1} is strictly related to the stretching vibration of Mo=*O*, whereas a maximum at 665 cm^{-1} refers to a triply coordinated bridging oxygen stretching mode of α-MoO_3. Furthermore, Raman modes that are located below 400 cm^{-1} are assigned to various bending vibrations and lattice modes of MoO_3[57,68]. For the last sample (AA450H), there are two intense peaks at about 400 cm^{-1}, which are characteristic of vibrations in MoS_2 molecules and are already described above. For samples (H) and (AA450H) the peaks indicating the presence of the trigonal phase of MoS_2 are not clearly seen, probably due to their smaller amount in the sample. Summing up, it can be stated that anodization causes the formation of an amorphous oxide layer, annealing generates crystalline MoO_3, whereas the hydrothermal process allows obtaining MoS_2 (from both the native oxide from anodization and the crystalline one).

The XRD patterns of the studied materials are shown in **Fig. S2** (Supplementary Information) and Fig. 2**o. Fig. S2** shows the whole pattern in the full range obtained for the prepared samples. Due to the fact that the performed synthesis leads to the deposition of thin layers directly on the surface of the current collector, the recorded signal comes mainly from the molybdenum substrate. However, when the diffractogram area between 10 and 50° is magnified, some signals may be distinguished, especially for the (AA450) sample. The results are consistent with the Raman spectroscopy, namely, the layer consists of MoO_3 [70–72]. Furthermore, for the Mo(A) and Mo(H) samples a signal at 39° from the molybdenum substrate may be identified. However, for the anodized sample, its intensity is relatively lower than for the sample that was not subjected to the anodization process. The reason is that the anodization process and subsequent modifications influence the crystal structure of molybdenum foil and thus the signal from the (110) plane fades [73], which is also visible in the XRD results of the other electrode materials. It can be simply explained by the growth of the film on the molybdenum surface, suggesting that this plane is privileged and the amorphous MoO_3 film is formed. Furthermore, the other samples seem to be characterized by an amorphous nature as the lack of signals may be observed. It is also worth noting that for the material's modifications that included a hydrothermal process, a weak signal at around 17° may be observed. However, due to the fact that the indicated signal is characterized by very low intensity, the authors note that this may only suggest the presence of MoS_2 as this is the value at which the (002) phase signal of 2H MoS_2 is usually observed [65,74–77]. It may also be stated that the broadening and low intensity are due to the ultrathin dimensions of MoS_2 and low crystallinity [78].

3.2. Electrochemical evaluation of the Mo-based electrode materials

In order to investigate the electrochemical performance of the electrode materials, cyclic voltammetry was applied. It is clearly seen in Fig. 3**a** that the widest potential range with electrochemical activity and with no occurrence of hydrogen reduction at cathodic scan, as well as the highest current density values were obtained for the Mo(AA450) electrode material, at least during the first few scans. It has to be mentioned that Mo(AA450) exhibits a drastic drop in electrochemical activity at the beginning of electrochemical tests and thus, the experiment performed at different scan rates was performed after several cycles in order to achieve some stability. It has already been reported that under repetitive charging and discharging, MoO_3 undergoes irreversible structure changes and as a result, poor kinetics and fast capacitance fading are observed [79–81]. Moreover, the cathodic limit of system stability is shifted towards more anodic potentials. Similar behavior was already shown and utilized for the modification of MoO_3-based electrodes for HER [82]. Cyclic voltammetry curves recorded at different scan rates for individual electrode materials are included in Supplementary Information (see **Fig. S3**, Supplementary Information). In order to investigate how the capacitance of each electrode material changes with a scan rate, cyclic voltammetry measurements with scan rates from 2 to 500 mV s^{-1} was performed, and the results are shown in Fig. 3**b**. For each material the capacitance was calculated according to Eq. (1) by analyzing the area under the CV curve, which is strictly related to the amount of charge stored by the electrode:

$$C = \int \frac{I(V)dV}{2v\ \Delta V} \tag{1}$$

Where $\int I(V)dV$ is the total voltammetric charge calculated by integration of positive and negative sweep in the potential window, v is a scan rate and ΔV is the potential window width. For the Mo(AA450) electrode material when increasing the scan rate, a rapid decrease in capacitance is observed, see Fig. 3**b**. This phenomenon can be due to the decomposition process of the electrode material and therefore its instability, especially observed when increasing the scan rate value. Moreover, at higher scan rates, the slower processes are kinetically hindered and cannot participate in a charge transfer onto or across the electrode/electrolyte interface, which is reflected by lower electrochemical capacitance [83–85]. The capacitance values of Mo (AA450) for the highest scan rates were even lower than for the Mo(AH) electrode material, which was also characterized by high capacitance values, especially in comparison with other molybdenum-based materials. Another advantage of the Mo(AH) may be observed in the EIS spectra, presented in Fig. 3**c**. Knowing that the reactance (Z'') can be described by Eq. (2)**:**

$$Z'' = -\frac{1}{2\pi fC} \tag{2}$$

where f is the frequency and C is the capacitance value, the Mo(AH) electrode material may offer the most promising capacitive properties. Also, the equivalent series resistance (ESR) is the parameter that may be

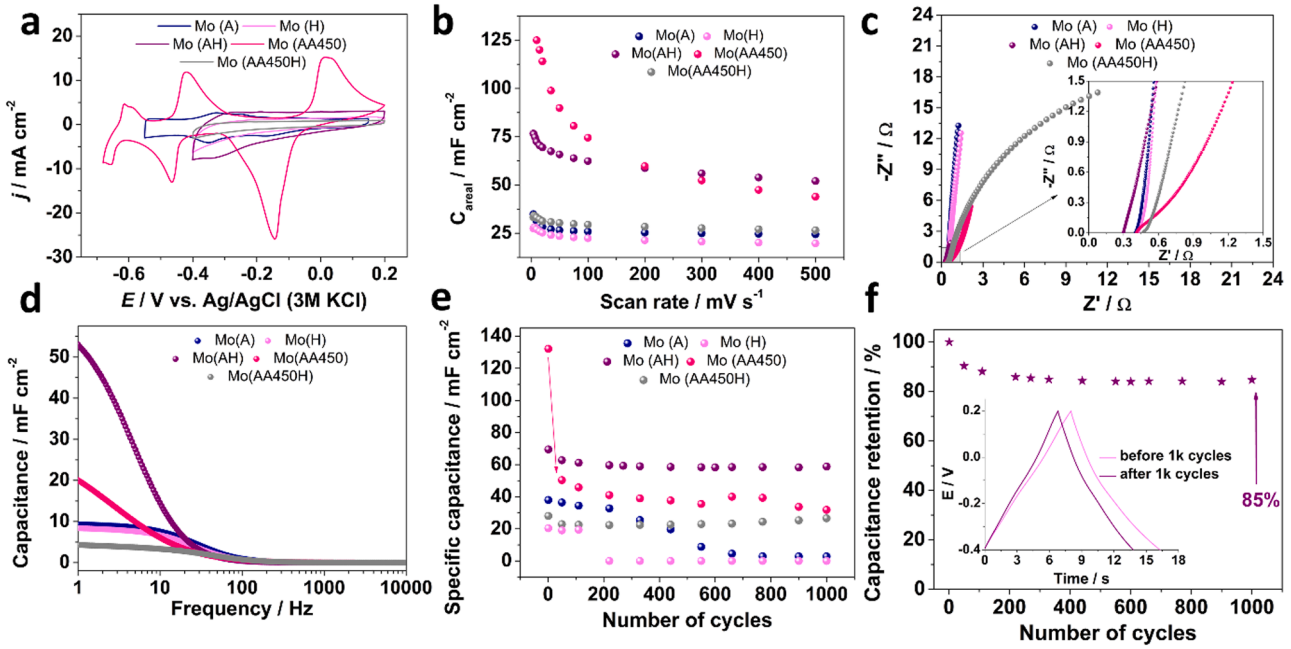

Fig. 3. a) CV curves recorded in 1 M H_2SO_4 ($\nu = 50$ mV s^{-1}) for Mo foil modifications; b) Areal capacitance in a function of a scan rate; c) Nyquist plots in a frequency range from 20 kHz to 100 mHz in 1 M H_2SO_4; d) specific capacitance in the function of applied frequency; e) Changes of specific capacitance during 1 000 cycles and f) changes of specific capacitance retention during 1 000 cycles for the Mo(AH) electrode material; inset: GCD curves before and after 1 000 cycles for the Mo(AH).

described as the intercept with the x-axis and its value depends not only on the electrolyte resistance, but also includes the electrode resistance and the contact resistance between the electrode material and the current collector [86]. Therefore, it may be concluded that the Mo(AH) electrode material is characterized by the lowest value of its internal resistance. Furthermore, a Nyquist plot for both (AA450) and (AA450H) materials in a low-frequency range has a flatter slope and therefore a smaller value of the phase angle, and in the high-frequency range, an appearance of a semi-circle forming might be observed, indicating that the charge transfer resistance arises and hinders the mobility of the ions [87]. A lack of the semicircle in the high-frequency range confirms that there is no ion adsorption/desorption on the electrode material surface coupled with electron transfer to the surface [88]. Moreover, especially in the case of Mo(A), Mo(H), and Mo(AH) electrode materials a line rising up vertically at a low-frequency range may be distinguished, pointing to the capacitive nature of the materials. However, the capacitance value for the Mo(AH) is considerably higher compared to other modifications (Fig. 3**d**) and the material is characterized by the best charge propagation in the range of very low frequencies, even lower than 1 Hz. Furthermore, capacitance values obtained from the electrochemical impedance spectroscopy measurements also confirm the loss of electrochemical activity of MoO_3 in the Mo(AA450) sample along with subsequent electrochemical measurements.

Initial charge and discharge measurements (GCD) were carried out for each material at different current densities applied (in a 3-electrode system). Prior to the cycling measurements, for each material the most optimal value for the applied current was selected, namely both charge and discharge time should be equal and not exceed 10 to 15 s – exemplary GCD curves are shown in Supplementary Information in **Fig. S4** (Supplementary Information). Then, at the selected current values, 1 000 charge and discharge cycles were performed, on the basis of which specific capacitances were calculated and presented in Fig. 3**e**. The results of GCD measurements are consistent with the cyclic voltammetry results presented above, especially when comparing the capacitance obtained at the 1st cycle with the values in Fig. 3**b**. The Mo(AA450) electrode material was characterized by the highest specific capacitance value, however, as the charging and discharging cycles progressed, a sharp decrease in capacitance was observed after the first 50 cycles, and capacitance retention after 1 000 cycles was just about 24%, see Fig. 3**e**. A rapid drop was also observed in the case of the Mo(H) electrode material (after 100 cycles), which was no longer characterized by capacitive properties. The loss of energy storage capacity is also seen in the case of molybdenum foil after anodization (Mo(A)). The highest capacitance retention was noticed for Mo(AA450H) which was at about 95%. However, for the Mo(AH) the capacitance value was even twice higher, namely 70 mF cm^{-2}, and the capacitance retention was at 85%, which is presented in Fig. 3**f**. Moreover, the inset in Fig. 3**f** shows that even after performing 1 000 charge-discharge cycles, a GCD curve preserved its triangular shape, without the increase of the ohmic drop.

With the aim to fully evaluate the electrochemical performance of the Mo(AH) electrode material and investigate the process of Pt-surface modification, an exceedingly large number of galvanostatic charge/discharge tests was performed with an initial value of current density of 4.5 mA cm^{-2} applied in the potential range from +0.2 V to −0.35 V. The cathodic potential limit was adjusted to −0.35 V in order to maintain the coulombic efficiency during cycles at the highest possible level. The resulting areal capacitance is presented in Fig. 4**a** and the inset shows the galvanostatic charge/discharge profile before (at 4.5 mA cm^{-2}) and after (at 34 mA cm^{-2}) 60 000 cycles. The results obtained up to 1 000 cycles are consistent with the ones presented above, while the phenomenon of a gradual increase in the value of the capacitance is observed during subsequent cycles, which is also confirmed by the inset in Fig. 4**a**, indicating an increase in both the charging and discharging time, while maintaining a shape that specifies capacitive properties. Due to the phenomenon of increasing capacitance, the value of applied current needed to be adjusted to maintain the appropriate charge/discharge time for supercapacitors, as well as to preserve a high level of coulombic efficiency during the subsequent cycles. Therefore, the current density was changed from 4.5 to 34 mA cm^{-2} which is presented in Fig. 4**a**. Furthermore, the gradual increase in the capacitance led to an increase in capacitance retention of around 1 000% after 60 000 cycles. Fig. 4**b** shows the value of coulombic efficiency, which remained at a very high level, averaging 100% during all cycles. The resulting capacitance increase was previously observed in the literature in the case of MoS_2-based electrode materials [43,44] and was e.g. explained by the activation process that takes place and enables the electrolyte

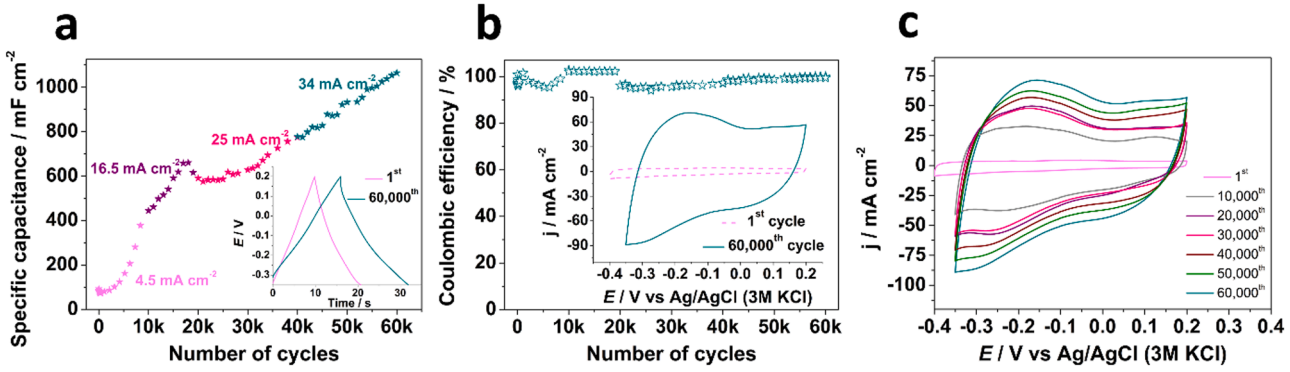

Fig. 4. a) Areal capacitance calculated on the basis of 60 000 GCD cycles for the Mo(AH) with the current adjustment during cycles; inset: GCD curves before and after 60 000 cycles, b) coulombic efficiency during 60 000 cycles; inset: CV curves before and after the measurements, c) CV curves for the Mo(AH) electrode material after subsequent cycles ($v = 50$ mV s^{-1}).

diffusion into the interlayers of MoS_2. Moreover, Fig. 4**c** presents the cyclic voltammetry curves after subsequent cycles, and it can be seen that the value of the current density increased significantly, especially in the negative potential range. As far as the authors are concerned, this is the highest capacitance value obtained for MoS_2-based electrode materials, but also one of the highest values for all supercapacitor materials.

3.3. Investigation of the increasing capacitance and the influence of the electrochemical dissolution-deposition process of Pt

In order to determine the cause of the constantly increasing capacitance and to investigate possible changes that took place in the morphology of the electrode material, additional SEM measurements were carried out after 15 000 charging and discharging cycles. As can be seen in Fig. 5**a-d**, the electrode's morphology after multiple charge/discharge cycles is markedly different from that of the Mo(AH) electrode material (see Fig. 1**g-h**). SEM images clearly show the delamination of the material, which is in striking contrast to that of the Mo(AH) before electrochemical measurements. In some previous studies [89–92] the electrochemical treatment has been demonstrated to be one of the techniques that leads to the exfoliation of the material. According to the literature, an exfoliated material is said to be characterized by a higher electrochemical capacitance compared to a bulk material [93–97]. Therefore, it may be concluded that the main cause of the increase in material's capacitance is the exfoliation process that takes place during the charge/discharge cycles. In fact, both of those effects were reported previously by Bissett et al. [44], finding the increase of the capacitance as a result of ion intercalation and partial exfoliation. The fact that the material may change during energy storage should be taken into account especially in the case of materials characterized by a layered structure with Van der Waals interactions, namely graphene and both transition metal oxides and dichalcogenides.

The SEM images obtained at higher magnification (see Fig. 5**b-d**) show changes that occurred in the electrode material during multiple charge/discharge cycles. In the structure of the material, one can observe particles embedded in the layer that were not present in the as-prepared material. The results of the EDS analysis (see **Fig. S5a**, Supplementary Information) and mapping results presented in Fig. 5**e-h** clearly indicate the presence of Pt particles embedded at the surface of the Mo(AH) electrode material. Even though the phenomenon of Pt dissolution-deposition has been discussed in a number of reports, still no universal mechanism describing the phenomenon was presented. Nevertheless, it may be assumed that the crucial parameter is the polarization potential of the Pt counter electrode. During galvanostatic charge/discharge cycles performed in a three-electrode configuration, the working electrode was cycled in the potential range from +0.2 to −0.35 V. Simultaneously, a potential of Pt CE was also recorded and one can see that it was polarized from 1.55 V to around −0.3 V (vs. Ag/AgCl

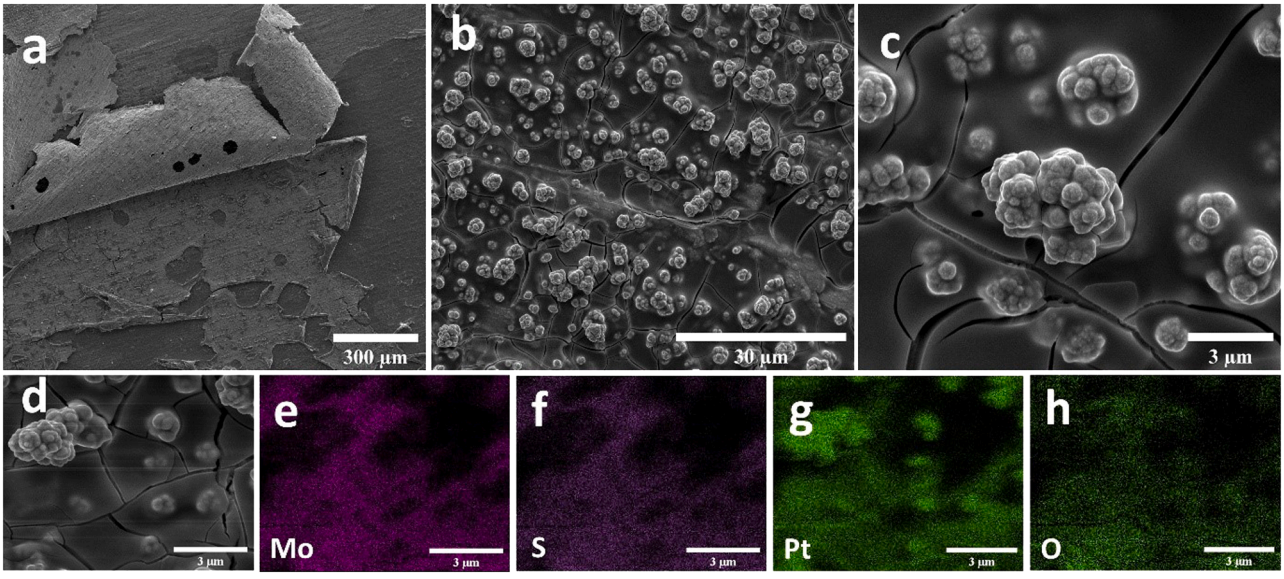

Fig. 5. a-c) SEM images and d-h) EDS mapping results for the Mo(AH) electrode material after 15 000 GCD cycles.

(3 M KCl) (see **Fig. S5b**, Supplementary Information). According to the literature reports, the oxidation and reduction of platinum occur principally after reaching high potential values during polarization, but the most intensified dissolution and deposition of Pt may occur during reversible cycling within a certain potential range, enabling repetitive oxidation and reduction of Pt [19,20,98]. Topalov et al. [99]. proposed that the oxidation of the Pt surface takes place about +1.15 V (vs. RHE) and as the potential value increases, the creation of a sub-surface oxide may occur, as well. The latter's presence is crucial during cathodic sweeping, as it contributes to the weakening of Pt–Pt bonds and as a consequence, during repetitive potential cycling, PtO_2 undergoes subsequent chemical and electrochemical dissolution [29]. Furthermore, oxygen atoms may distort the surface lattice through tunneling into the deeper layers and triggering the dissolution [100,101]. As a result, both Pt^{2+} and Pt^{4+} ions are generated, according to Eqs. (3) and (4):

$$PtO_{2(s)} + 4H_{(aq)}{}^{+} + 2e^{-} \rightarrow Pt^{2+}{}_{(aq)} + 2H_2O \quad (3)$$

$$PtO_{2(s)} + 4H^{+}{}_{(aq)} \rightarrow Pt^{4+}{}_{(aq)} + 2H_2O \quad (4)$$

To the best of our knowledge, this is the first time when the phenomenon is observed in the electrochemical measurements performed for electrode materials with the application for energy storage in supercapacitors. The reason for this may be both the fact that, in the case of the analyzed electrode material very high current densities are obtained, as well as the fact that there is little research in the literature on electrode materials for supercapacitors that thoroughly investigate the changes taking place in the material during multiple charge/discharge cycles. Therefore, bearing in mind Wei's et al. critical approach to the use of platinum electrode in HER measurements[30], authors would like to emphasize that when a Pt counter electrode is used in the study of energy storage materials, careful consideration should be given to the investigation, as well. Therefore, in order to make sure whether the incorporation of platinum into the material affects its overall performance, galvanostatic charge/discharge tests were performed with the separation of the working electrode from the counter electrode, and the results are presented in **Fig. S6**. Based on all the results presented above, the Mo(AH) material with Pt-surface modification was further investigated and from this moment, it was designated as Pt@1T/2H-MoS_2, whereas the electrode material that was not subjected to the Pt-modification was designated as 1T/2H-MoS_2.

The obtained results indicate, that despite the absence of Pt on the surface of the working electrode, an increase in capacitance is still observed, but it is almost two times smaller than in the case of dissolution and deposition of platinum (**Fig. S6a**). Moreover, no matter how the measurement system was designed, the electrode material still has an almost ideal coulombic efficiency (**Fig. S6b**), and the GCD curves retain a triangular shape (inset of **Fig. S6a**). The phenomenon of increasing capacitance is also confirmed by the EIS results presented in **Fig. S6c**. A slightly increasing slope of the curves indicates an improving capacitive behavior [102], while a gradually decreasing value of the imaginary element of impedance additionally confirms these observations, in accordance with Eq. (2). The absence of platinum on the surface of the electrode material was confirmed by SEM and XPS analysis performed after 15 000 charge-discharge cycles (see **Fig. S7**, Supplementary Information). The chemical composition of the sample remained almost unchanged, only the presence of traces of SO_4^{2-} was observed. In the case of the morphology of the surface, moss-like nanostructures are still present and visible as before the cycles, but the surface has become more solid with numerous cracks. However, the obtained results may indicate that the process of dissolution-deposition of Pt significantly contributes to the acceleration of the activation process which results in a greater increase in the capacitance. On the other hand, when platinum is not present in the solution and thus the deposition does not occur, the activation process is slower. However, it can undoubtedly be said that Pt-assisted activation of the electrode material is beneficial in the energy storage process.

For further analysis of the capacitance increase and a more thorough investigation of the Pt-surface modification, XPS analysis was performed in order to investigate the changes occurring in the Pt@1T/2H-MoS_2 electrode material during long-term cycles. As shown in Fig. 6, for the electrode material before cycles (0th) the Mo 3*d* spectrum shows that it is possible to distinguish two polymorphs of MoS_2, as it was confirmed with Raman spectroscopy results and described in the first part of the manuscript. With subsequent cycles, one can observe more intense peaks coming from Mo^{6+} at 233.3 and 236.4 eV [37] and a new pair of doublets coming from Mo^{5+} assigned to the peaks at 231.8 and 235.2 eV [39,103,104] (see spectrum after 3 000 cycles). The results indicate a decreasing and finally completely disappearing presence of both 1T and 2H-MoS_2 (see spectrum after 21 000 cycles). The transition of both 1T and 2H-MoS_2 into mixed non-stoichiometric molybdenum oxides also confirms the spectrum recorded for S2p, showing that with the successive cycles, S^{2-} is converted to SO_4^{2-} [39] (see **Fig. S8**, Supplementary Information). XPS analysis also confirmed the presence of platinum in the electrode material, mainly in the metallic form, but also small amounts of Pt^{2+} and Pt^{4+} were observed (see **Fig. S8**, Supplementary Information). Moreover, in the first part of repetitive cycling, one may see the increase of peaks assigned to Mo^{6+}. According to the literature reports, a metal/metal oxide interaction should also be taken into consideration as it influences the conductivity and metal oxide's reactivity[103]. Small amounts of Mo^{6+} that are present in the sample after synthesis, probably related to the anodization carried out in the first stage of the synthesis, are reduced in contact with the metal substrate, and the metal is oxidized, which may also contribute to the increased amount of metal oxides observed in the material. Furthermore, with the increasing number of repetitive cycles, the amount of molybdenum oxides is increased at the expense of molybdenum sulfide, which is confirmed by XPS results after subsequent cycles as the dominance of molybdenum in the 5+ and 6+ oxidation state can be observed. With the elongation of galvanostatic measurements, the presence of reduced forms of molybdenum is noted – Mo^{4+} at 231.2 and 234.5 eV[105], as well as $Mo^{\delta+}$ at 229.5 and 232.6 eV. $Mo^{\delta+}$relates to the oxidation states $0 < \delta < 4$ and may be related with the presence of oxygen vacancies in MoO_2 lattice [106,107]. Furthermore, as it was stated by Grainer et al., Mo^{5+} cations are also formed as a result of oxygen vacancy defects in MoO_3, and after a certain vacancy concentration is reached, Mo^{4+} cations develop [103,104]. Despite the appearance of molybdenum in the 4+ oxidation state, it is not a signal from the original MoS_2 compound, as no signal indicating the presence of sulfur was registered again, which indicates the formation of only oxygen compound of molybdenum (MoO_x) with mixed valence states. Furthermore, on the basis of the Mo-O phase diagram it can be stated that MoO_3 is not expected to equilibrate directly with Mo at Mo/MoO_3 interface, but the equilibrium may be reached between Mo and MoO_2 [108]. There are also several intermediate, non-stoichiometric molybdenum oxides with mixed oxidation states that may be stable in between MoO_3 and Mo. On this basis it may be concluded the results obtained after a major number of cycles are consistent with that, as we observe diminishing intensity of peaks related to Mo^{6+} and Mo^{5+} at the expense of lower oxidation states. Furthermore, in several reports it was stated that when Mo^{6+} is dominant in the sample, a material is characterized by a poorer conductivity, and with its subsequent reduction, the Mo 4d states that were empty are being filled with electrons, resulting in the increased conductivity [40,42,102,104]. Carrying out subsequent cycles consistently increased the intensity of signals from forms on lower oxidation states, which is in agreement with the continually increasing capacitance.

Furthermore, the morphology of Mo(AH) electrode material before and after repetitive cycles was investigated using transmission electron microscopy and the results are presented in Fig. 7. The results for the sample before cycles (Fig. 7**a-c**) confirm the morphology observed at SEM images, namely curled nanoflake-like structure may be distinguished that is mainly amorphous. However, the crystalline structure of

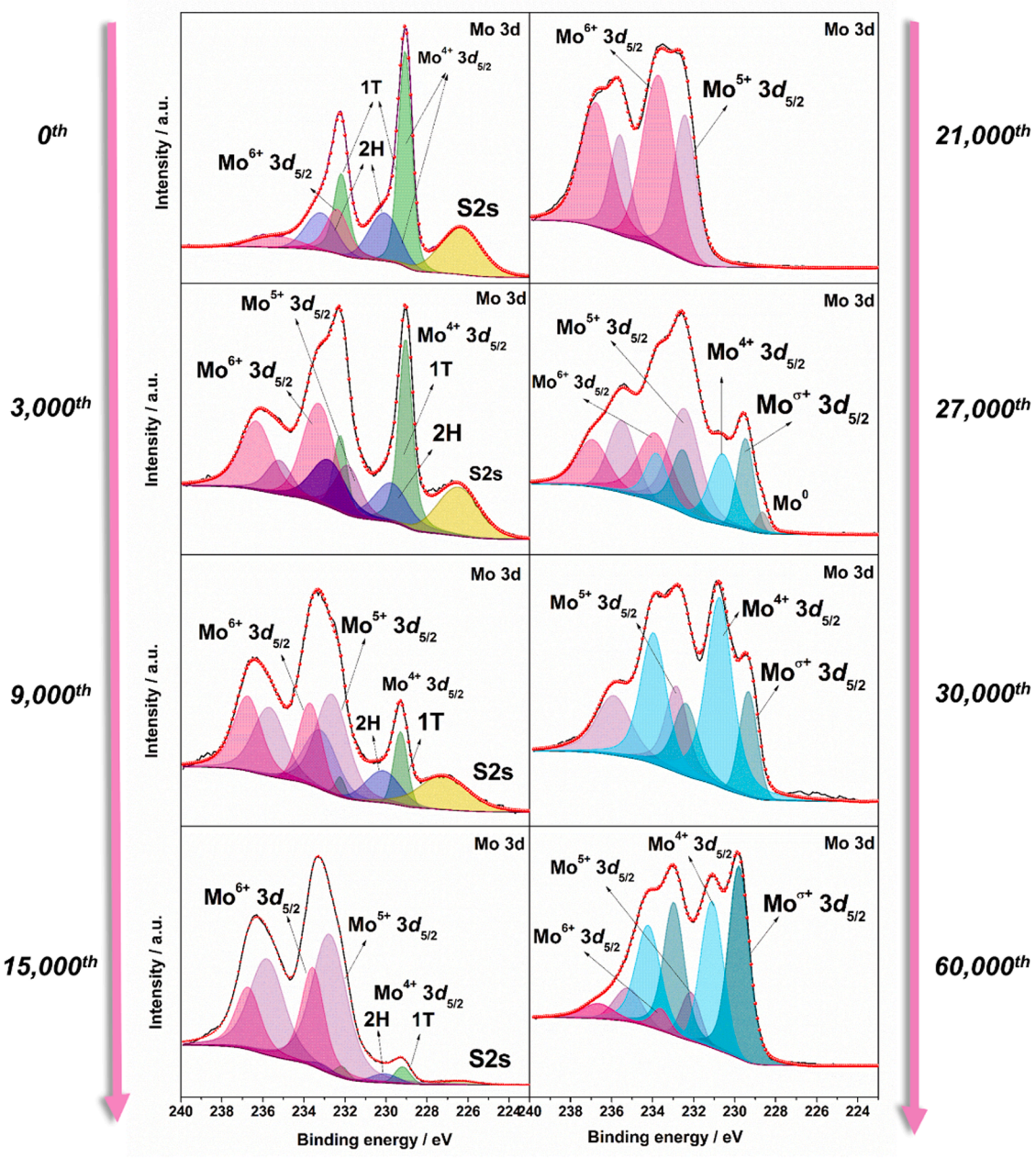

Fig. 6. XPS spectra of Mo 3d for the Pt@1T/2H-MoS_2 electrode material before and after subsequent (3, 9, 15, 21, 27, 30 and 60k) GCD cycles with Pt-surface modification.

MoS_2 may be observed on the edges of the structure, as well. For the Pt@1T/2H-MoS_2 material after 30 000 cycles, the results exhibit the presence of Pt particles in Pt@1T/2H-MoS_2 electrode material occurring as darker spots, which was also confirmed by EDS analysis (see Fig. 7**d-f**). What is more, when the cycles were performed with the separated WE and CE areas (see Fig. 7**g-i**), the morphology more closely resembles the one observed before the cycles.

3.4. *Charge storage mechanism analysis*

In order to properly classify the electrode material being used, it is essential to determine the mechanism through which the charge is being stored. One of the approaches to differentiate capacitances was firstly presented by Conway et al. [109]. and followed by its application by Dunn et al. to analyze the charge storage mechanism of nanostructured transition metal oxides [110–112]. This method allows for quantitive separating the contribution of the surface-confined elements from the diffusion-controlled processes responsible for charge storage by assuming that the total current response at a specified potential ($i(V)$) is the sum of the current related to surface controlled and diffusion-limited processes, according to the following Eq. (5):

$$i(V) = k_1 v + k_2 v^{1/2} \tag{5}$$

where $i(V)$ represents a measured current, k_1 and k_2 are constant values, and v is a scan rate. After transforming Eq. (5) to the form of Eq. (6), the obtained linear dependence with the slope (k_1) and Y-intercept (k_2) values enables to determine the contribution of the outer surface ($k_1 v$) and inner surface ($k_2 v^{1/2}$) to the total charge being stored at a given potential:

$$\frac{i(V)}{v^{1/2}} = k_1 v^{1/2} + k_2 \tag{6}$$

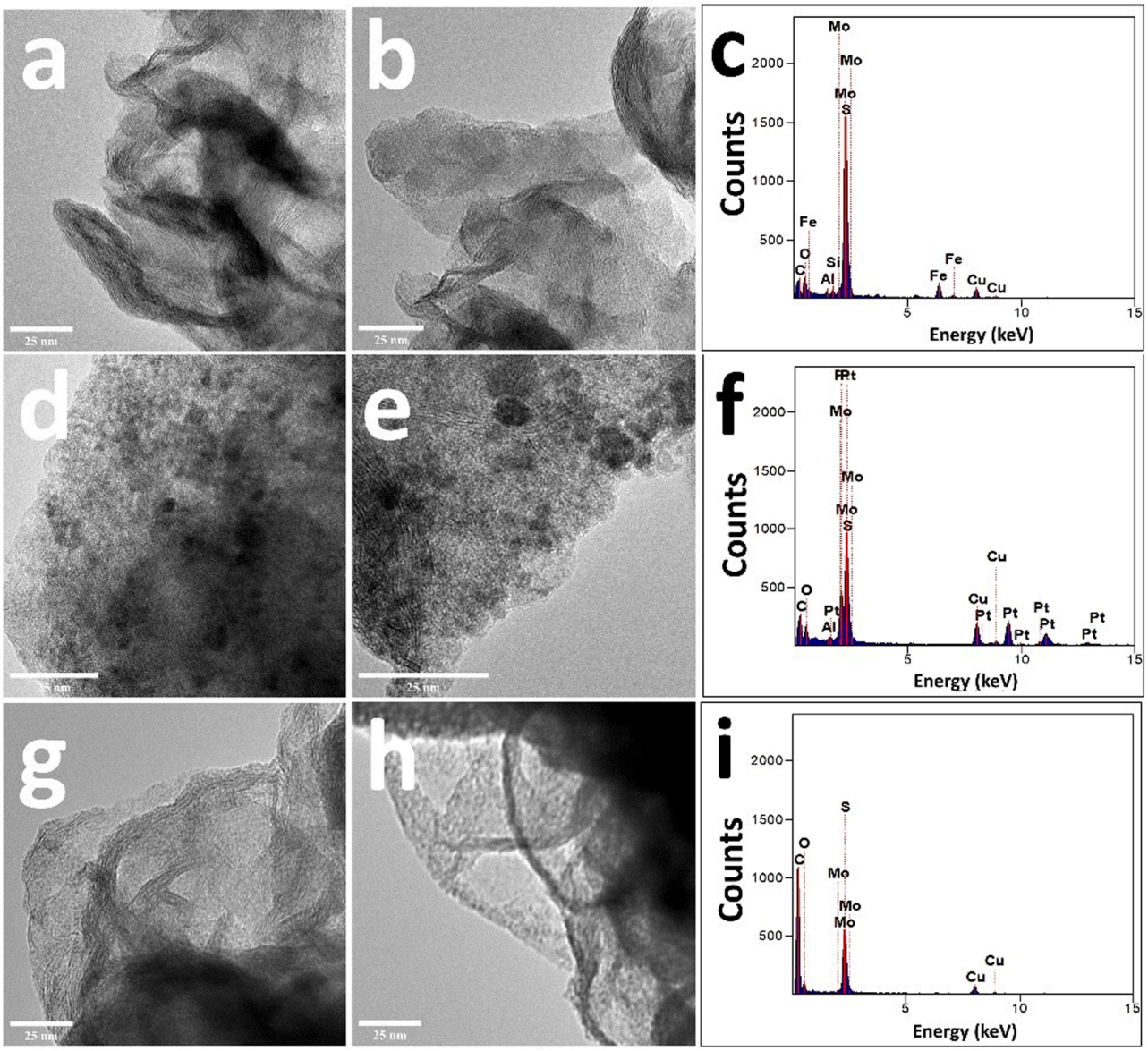

Fig. 7. TEM images and EDS spectra of a-c) Mo(AH), d-f) Pt@1T/2H-MoS_2 after 30 000 cycles and g-i) 1T/2H-MoS_2 after 30 000 cycles.

Fig. S9 shows the results of the Dunn's method application for the analysis of the Mo(AH) charge storage mechanism (before modification with Pt particles), namely cyclic voltammetry curves carried out at different scan rates in the range from 10 to 500 mV s^{-1} are presented. It can be noticed that when the scan rate value increases, the increase in the surface-controlled contribution is observed and it remains at a high level with the increasing scan rate applied. To analyze in detail how and whether Pt-doping affects the energy storage mechanism, the presented approaches of differentiating capacitances were used for both Pt@1T/2H-MoS_2 and 1T/2H-MoS_2 electrode materials during repetitive cycling.

Another method of differentiating capacitances was proposed by Trasatti and coworkers [113] stating that it is possible to estimate the contribution of diffusion-controlled and surface-controlled charge to the overall charge being stored, according to Eq. (7):

$$q_T = q_i + q_o \tag{7}$$

where q_T is the total amount of charge, q_i represents the charge stored at the "inner" surface and q_o is the charge stored at the "outer" surface. The proposed approach is based on the fact that charge storage at the outer electrode surface is independent of the scanning rate, whereas the process of charge storage at the inner surface is controlled by diffusion. Performing cyclic voltammetry at different scan rates and evaluating corresponding areal capacitances constitute a base to investigate capacitive contribution from electrical double layer and pseudo-capacitive reactions. Assuming that the diffusion of ions follows a semi-infinite pattern, it should be possible to observe a linear relationship between the reciprocal of the calculated areal capacitance (C^{-1}) and the square root of the scan rate ($v^{1/2}$), according to Eq. (8):

$$C^{-1} = const \cdot v^{1/2} + C_T^{-1} \tag{8}$$

where C_T is a total capacitance, namely the sum of pseudo-capacitance and electric double layer capacitance. Furthermore, plotting the capacitance (C) versus the reciprocal of the scan rate allows to estimate the value of the contributed capacitance of the electrical double layer (C_O), according to Eq. (9):

$$C = const \cdot v^{-1/2} + C_O \tag{9}$$

Eventually, subtracting C_O from C_T results in a determination of maximum pseudo-capacitance value. The evaluation of the contribution of the Mo(AH) electrode material before galvanostatic charge/discharge

tests is presented in Fig. 8**a,b**, whereas the final results are compared with Dunn's analysis in Fig. 8**c**. The values were obtained from a linear fit within the restricted range of the scan rate – the rest of the polarization range was disregarded due to the high ohmic drop caused by the electrode material's internal resistance.

It is clearly seen in Fig. 8**c** that even though the non-diffusive contribution is higher for the Dunn's analysis, especially for the higher scan rates. The trend towards an increase of surface-controlled contribution may also be observed in the case of the highest scan rates, for which the differentiation of the capacitance was carried out using Dunn's method and the outer surface contribution reaches 94% (see **Fig. S9**, Supplementary Information). Processes responsible for energy storage reactions can be expressed as shown below in Eq. (10) [114, 115]:

$$(MoS_2)_{surface} + H^+ + e^- \rightarrow \left(MoS_2^- H^+\right)_{surface} \quad (10)$$

On the other hand, as mentioned above, a layered structure allows ions to intercalate, which results in a contribution of a pseudocapacitance similar to a battery-type one [116], but often wrongly confused with it. According to the literature and both empirical studies and mathematical models presented therein, in the case of 2H-MoS_2 electrode materials, it is necessary to provide a high voltage value that would allow the transfer of electrons through a wide band gap in order to fill the unoccupied states of 2H-MoS_2 and hence contributing to the increasing pseudocapacitance contribution [117]. Therefore, the 2H phase is mainly characterized by EDL capacitive properties, especially in aqueous electrolytes. On the contrary, 1T-MoS_2 is able to store charge using both EDL and pseudocapacitive mechanisms. According to the literature, reversible redox reactions may occur at a large density of states, namely a significant number of d-orbitals of molybdenum atoms above the Fermi level may be observed. For both crystallographic phases, pseudocapacitance's occurrence is mainly due to Mo-edge activity [17,117]. Furthermore, the cyclic voltammetry curves (see **Fig. S3**, Supplementary Information) clearly show the combination of nearly rectangular shape and pseudocapacitive behavior, and the latter may be depicted as follows in Eq. (11):

$$MoS_2 + xe^- + xH^+ \rightarrow (MoS - SH) \quad (11)$$

For the 1T/2H-MoS_2 electrode material, the results of Dunn's and Trasatti's analysis after 15 000 and 30 000 cycles are presented in **Fig. S10** (Supplementary Information, with the CE and WE areas separated). The obtained results indicate that with the successive charging and discharging cycles, we do not observe such significant changes in the energy storage mechanisms. As with the original material, energy is mainly stored through the formation of an electrical double layer. The conclusions are consistent with the previously presented observations that the composition of the material does not change and neither does the energy storage mechanism. On the other hand, for the Pt@1T/2H-MoS_2, as it was stated above, during the repetitive cycling and simultaneous Pt-modification, the change in the chemical composition of electrode material may be observed, and thus a change in the energy storage mechanism. Consequently, with the increasing number of cycles, an increase in the diffusion-controlled contribution is observed (see Fig. 8**d,e**). The results are consistent with the presented XPS results, which indicate that the material is transformed into mixed molybdenum oxides MoO_x. Transition metal oxides, including molybdenum oxides, are characterized by pseudocapacitive properties and it has been already reported that oxygen-deficient MoO_x with varieties of oxidation states are particularly promising for energy storage applications [40,118,119]. Therefore, due to its enhanced overall electrochemical performance, the Pt@1T/2H-MoS_2 electrode material obtained after 10 000 repetitive charge/discharge cycling was tested in a two-electrode system.

3.5. Two electrode configuration measurements

The results of the two-electrode measurements for the Pt@1T/2H-MoS_2 electrode material obtained after 10 000 repetitive charge/discharge cycling are presented in Fig. 9. The electrode material in the two-electrode configuration was subjected to 50,000 charge/discharge cycles with an applied voltage of 0.6 V and a flowing current of 11.9 mA cm^{-2}. In Fig. 9**a**, it can be seen that the capacitance remains stable, and the value of which does not decrease with time. Moreover, a slight

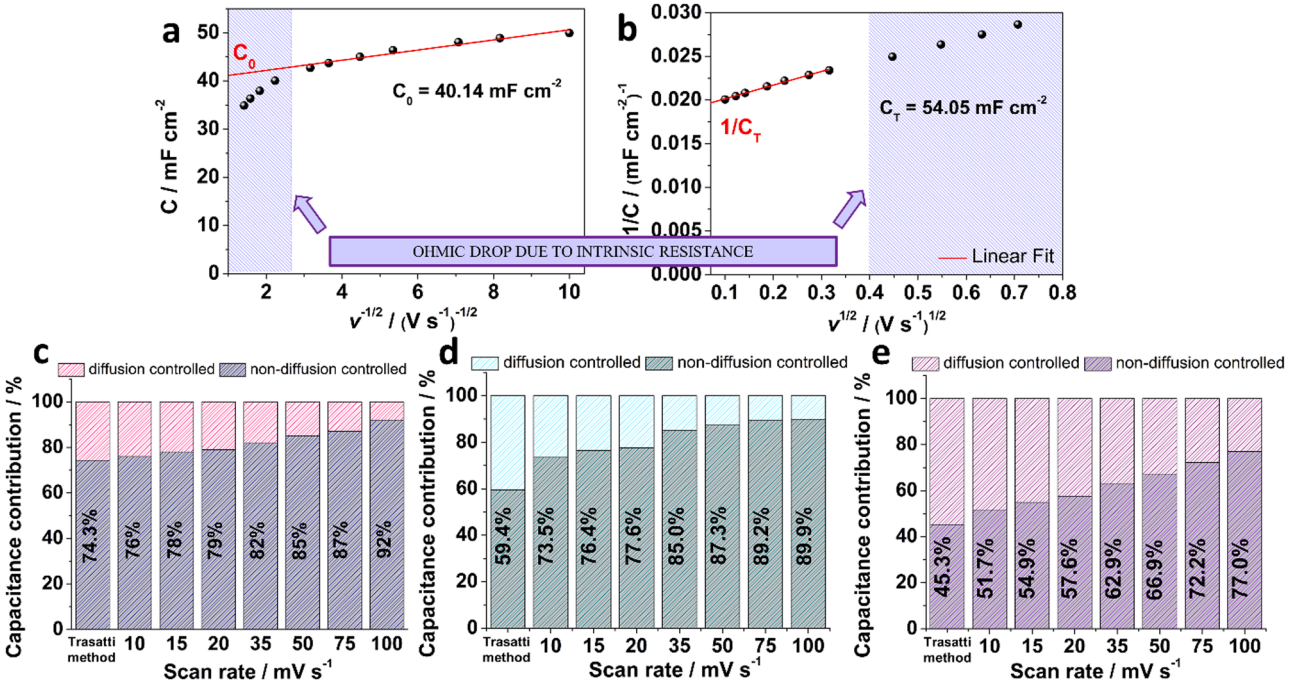

Fig. 8. Determination of a) outer surface capacitance contribution (C_O) and b) total capacitance (C_T) for Mo(AH) before Pt-surface modification, based on Trasatti method; comparison of the results from Trasatti method and Dunn's method c) before Pt-surface modification, d) after 15 000 cycles (Pt@1T/2H-MoS_2) and e) after 30 000 cycles of repetitive cycling (Pt@1T/2H-MoS_2).

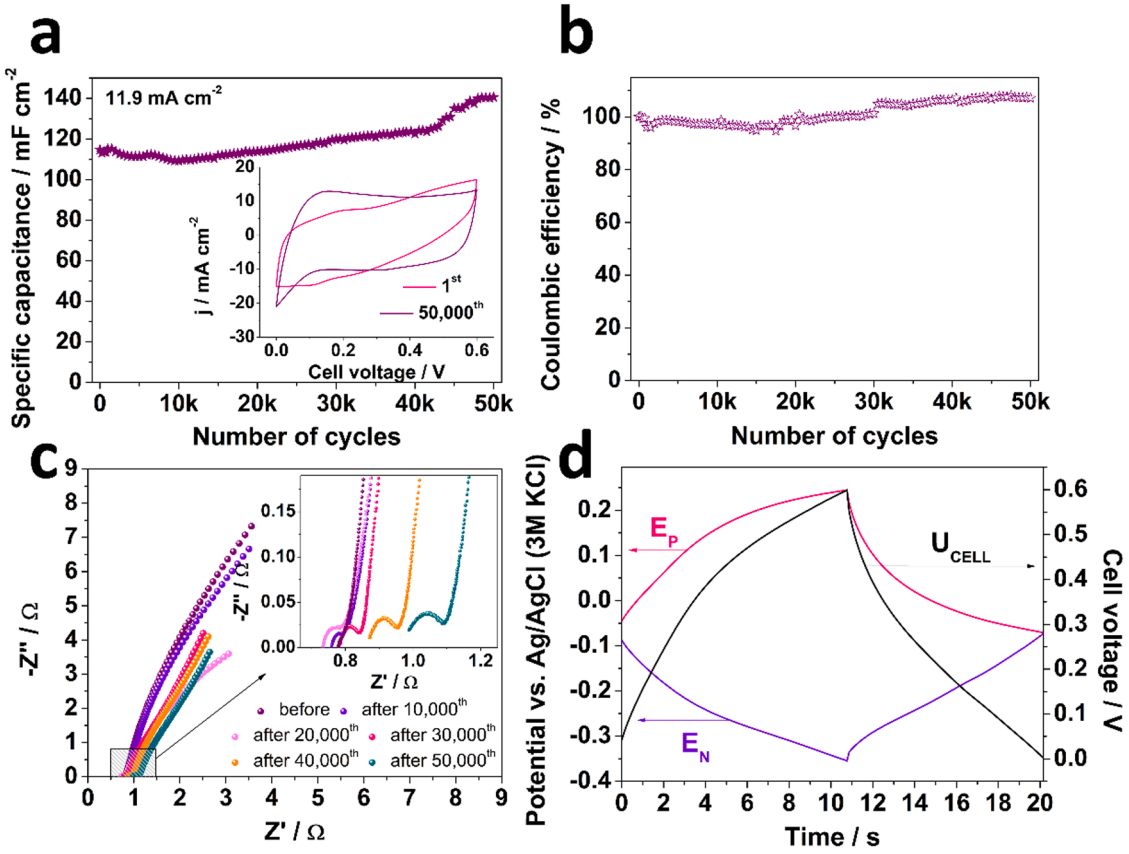

Fig. 9. a) Areal capacitance of the Pt@1T/2H-MoS_2 symmetric supercapacitor calculated on the basis of 50 000 GCD cycles (inset: CV curves before and after 50 000 cycles); b) coulombic efficiency after 50 000 cycles; c) EIS results during subsequent cycles in the frequency range between 20 kHz and 100 mHz; d) galvanostatic charge/discharge profile for the Pt@1T/2H-MoS_2 symmetric supercapacitor.

increase in capacitance was recorded with the increasing number of cycles performed, which is probably due to the still occurring, albeit to a smaller extent, intercalation process and the complementary changes in the electrode material. The increase in capacitance is also visible in the inset provided, showing the recorded voltammetry curves before and after 50 000 cycles. The material in the symmetric supercapacitor system was also characterized by a high-reaching coulombic efficiency during multiple cycles (Fig. 9**b**) and unprecedented capacitance retention (120% after 50 000 cycles), and it was recorded that by applying a voltage of 0.6 V it is distributed almost symmetrically over both electrode materials (Fig. 9**d**). Electrochemical impedance spectroscopy analysis was also performed during the repetitive cycling and the results are shown in Fig. 9**c**. It can be observed that before the measurements, the impedance curve was a straight line, also in the higher frequency range, indicating capacitive properties. Along with the subsequent cycles, in the high-frequency range, a semicircle can be distinguished, pointing to the increasing resistance associated with the charge transfer processes. Furthermore, the appearance of the semicircle in the high-frequency range confirms that an ion adsorption/desorption on the electrode material surface coupled with electron transfer to the surface takes place [88]. There is also a noticeable shift of the intersection with the x-axis value towards higher ones, suggesting an increase in the equivalent series resistance. Nevertheless, at each stage of the repetitive cycling, the overall resistance is small, indicating the good conductivity of the electrode. Moreover, for a comparison, multiple charge/discharge cycles were also performed for the 1T/2H-MoS_2 electrode material without Pt surface modification (see **Fig. S11**, Supplementary Information). In this case, an increase in the capacitance was also observed, as well as an almost perfect coulombic efficiency, as in the case of materials in a three-electrode configuration cell. However, for the material that was not modified with Pt particles, the values of the recorded capacitance were much smaller, and therefore the supercapacitor was working at lower current values and the operating voltage value was lower. Nevertheless, Pt@1T/2H-MoS_2 symmetric supercapacitor was primarily characterized by unprecedented capacitance retention, with no significant degradation of the electrode material. A comparison with current literature data on Mo-based electrode materials for supercapacitors is provided in **Table S1** (Supplementary Information).

4. Conclusions

The investigation of the different approaches for the synthesis of MoS_2 electrode material was performed, including anodization, hydrothermal process, and annealing, with the results indicating that depending on the processes carried out, amorphous molybdenum oxide, amorphous molybdenum sulfide or crystalline molybdenum oxide is obtained. The electrode material prepared via anodization of a molybdenum plate, followed by a hydrothermal process in thiourea aqueous solution was obtained in a form of a thin layer on metallic molybdenum substrate. The electrode material was characterized by the increasing capacitance during subsequent cycles, which was strictly related to the platinum dissolution-deposition process that occurred during repetitive cycling in 1 M sulfuric acid with Pt acting as a counter electrode. The analysis of the Pt-surface modification during multiple charging and discharging cycles revealed that Pt-surface modification happening simultaneously with the H^+ ions intercalation resulted in boosting the exfoliation process, and as a result, the increase of capacitance was higher in comparison with non-modified MoS_2. After 60 000 cycles, the specific capacitance of the Pt@1T/2H-MoS_2 electrode material increased to over 1 F cm^{-2}, with the coulombic efficiency above 97%

during all the cycles. Furthermore, this study revealed that upon Pt-surface modification, the material's composition has been changed. XPS analysis revealed that the transition to mixed molybdenum oxides took place altogether with the introduction of oxygen vacancies into the structure. Altogether with the platinum deposition, significant changes in the energy storage mechanism were observed. Pt-modified electrode material was characterized by a greater contribution of pseudocapacitance in the charge storage processes, which was increasing with the greater number of cycles applied. The phenomenon was strictly related to the presence of mixed molybdenum oxides on the surface and thus, such a modified material was used for the symmetric two-electrode configuration with the capacitance reaching 140 mF cm^{-2} after 60 000 galvanostatic cycles and the coulombic efficiency at around 100% during all cycles.

The authors also believe that the conclusions drawn and the observations presented are a noteworthy and profound insight that provides a novel approach for understanding the ongoing processes taking place in the measurement system, especially when the counter electrode for electrochemical measurements is considered. Furthermore, the authors are of the opinion that paying attention to the constant variability of the material during charge-discharge processes, resulting in electrochemical but also physicochemical changes, can certainly help in gaining in-depth knowledge about the mechanisms underlying energy storage by electrode materials. We also believe that careful consideration should be taken into account when Pt counter electrode is used in the study of energy storage materials due to the dissolution-deposition phenomenon of platinum, which, may have a positive effect on the overall electrochemical performance of the electrode material, should not be ignored regardless of the circumstances. Nevertheless, the results indicate that Pt-surface modification of MoS_2 may provide a novel approach for electrode materials for high-performance supercapacitors.

Credit author statement

Zuzanna Zarach: Conceptualization, Methodology, Validation, Formal analysis, Investigation, Writing - Original Draft, Writing - Review & Editing, Visualization, Project administration; **Mariusz Szkoda**: Conceptualization, Methodology, Validation, Writing - Original Draft, Writing - Review & Editing, Supervision, Project administration, Funding acquisition; **Konrad Trzciński**: Conceptualization, Methodology, Writing - Review & Editing; **Marcin Łapiński**: Investigation, Resources; **Grzegorz Trykowski**: Investigation, Resources, Writing - Original Draft, Visualization; **Andrzej P. Nowak**: Conceptualization, Validation, Formal analysis, Writing - Review & Editing, Supervision

Declaration of Competing Interest

The authors declare the following financial interests/personal relationships which may be considered as potential competing interests.

Data availability

Data will be made available on request.

Acknowledgments

This work was supported by The National Centre for Research and Development (Grant no LIDER/15/0088/L-10/18/NCBR/2019). We thank K. Jurak for providing the access to the X-ray Photoelectron Spectroscopy apparatus. We would also like to thank M. Gazda for assistance with X-diffraction pattern measurements, and M. Sawczak who provided the access to the micro-Raman spectrometer.

Supplementary materials

Supplementary material associated with this article can be found, in the online version, at doi:10.1016/j.electacta.2022.141389.

References

[1] D. Saha, P. Kruse, Editors' choice—review—conductive forms of MoS2 and their applications in energy storage and conversion, J. Electrochem. Soc. 167 (2020), 126517, https://doi.org/10.1149/1945-7111/ABB34B.
[2] T. Wang, H.C. Chen, F. Yu, X.S. Zhao, H. Wang, Boosting the cycling stability of transition metal compounds-based supercapacitors, Energy Storage Mater. 16 (2019) 545–573, https://doi.org/10.1016/J.ENSM.2018.09.007.
[3] D. Kong, H. He, Q. Song, B. Wang, W. Lv, Q.-H. Yang, L. Zhi, Rational design of MoS 2 @graphene nanocables: towards high performance electrode materials for lithium ion batteries, Energy Environ. Sci. 7 (2014) 3320–3325, https://doi.org/10.1039/C4EE02211D.
[4] B. Yao, L. Huang, J. Zhang, X. Gao, J. Wu, Y. Cheng, X. Xiao, B. Wang, Y. Li, J. Zhou, Flexible transparent molybdenum trioxide nanopaper for energy storage, Adv. Mater. 28 (2016) 6353–6358, https://doi.org/10.1002/ADMA.201600529.
[5] Z. Dai, W. Jin, M. Grady, J.T. Sadowski, J.I. Dadap, R.M. Osgood, K. Pohl, Surface structure of bulk 2H-MoS2(0001) and exfoliated suspended monolayer MoS2: a selected area low energy electron diffraction study, Surf. Sci. 660 (2017) 16–21, https://doi.org/10.1016/J.SUSC.2017.02.005.
[6] W. Xu, C. Sun, K. Zhao, X. Cheng, S. Rawal, Y. Xu, Y. Wang, Defect engineering activating (Boosting) zinc storage capacity of MoS2, Energy Storage Mater. 16 (2019) 527–534, https://doi.org/10.1016/J.ENSM.2018.09.009.
[7] L. Miao, Z. Song, D. Zhu, L. Li, L. Gan, M. Liu, Recent advances in carbon-based supercapacitors, Mater. Adv. 1 (2020) 945–966, https://doi.org/10.1039/D0MA00384K.
[8] L. Lin, W. Lei, S. Zhang, Y. Liu, G.G. Wallace, J. Chen, Two-dimensional transition metal dichalcogenides in supercapacitors and secondary batteries, Energy Storage Mater. 19 (2019) 408–423, https://doi.org/10.1016/J.ENSM.2019.02.023.
[9] H. Liu, X. Liu, S. Wang, H.K. Liu, L. Li, Transition metal based battery-type electrodes in hybrid supercapacitors: a review, Energy Storage Mater. 28 (2020) 122–145, https://doi.org/10.1016/J.ENSM.2020.03.003.
[10] C. Liu, Y. Bai, Y. Zhao, H. Yao, H. Pang, MoS2/graphene composites: fabrication and electrochemical energy storage, Energy Storage Mater. 33 (2020) 470–502, https://doi.org/10.1016/J.ENSM.2020.06.020.
[11] Y.C. Lin, D.O. Dumcenco, Y.S. Huang, K. Suenaga, Atomic mechanism of the semiconducting-to-metallic phase transition in single-layered MoS2, Nat. Nanotechnol. 9 (2014) 391–396, https://doi.org/10.1038/nnano.2014.64, 2014 95.
[12] L. Hu, X. Shan, Y. Wu, J. Zhao, X. Lu, Laser thinning and patterning of MoS2 with layer-by-layer precision, Sci. Rep. 7 (2017) 1–9, https://doi.org/10.1038/s41598-017-15350-4, 2017 71.
[13] R. Kappera, D. Voiry, S.E. Yalcin, B. Branch, G. Gupta, A.D. Mohite, M. Chhowalla, Phase-engineered low-resistance contacts for ultrathin MoS2 transistors, Nat. Mater. 13 (2014) 1128–1134, https://doi.org/10.1038/nmat4080, 2014 1312.
[14] D. Sarkar, D. Das, S. Das, A. Kumar, S. Patil, K.K. Nanda, D.D. Sarma, A. Shukla, Expanding interlayer spacing in MoS2 for realizing an advanced supercapacitor, ACS Energy Lett. 4 (2019) 1602–1609, https://doi.org/10.1021/ACSENERGYLETT.9B00983/SUPPL_FILE/NZ9B00983_SI_001.PDF.
[15] R.B. Pujari, A.C. Lokhande, A.R. Shelke, J.H. Kim, C.D. Lokhande, Chemically deposited nano grain composed MoS2 thin films for supercapacitor application, J. Colloid Interface Sci. 496 (2017) 1–7, https://doi.org/10.1016/J.JCIS.2016.11.026.
[16] A.S. Neetika, V.K. Malik, R. Chandra, One step sputtered grown MoS2 nanoworms binder free electrodes for high performance supercapacitor application, Int. J. Hydrog. Energy 43 (2018) 11141–11149, https://doi.org/10.1016/J.IJHYDENE.2018.05.005.
[17] M. Acerce, D. Voiry, M. Chhowalla, Metallic 1T phase MoS2 nanosheets as supercapacitor electrode materials, Nat. Nanotechnol. 10 (2015) 313–318, https://doi.org/10.1038/nnano.2015.40, 2015 104.
[18] R.M. Cerviño, W.E. Triaca, A.J. Arvia, Electrochemical preparation and characteristics of platinum electrode surfaces with preferred orientations, J. Electroanal. Chem. Interfacial Electrochem. 182 (1985) 51–60, https://doi.org/10.1016/0368-1874(85)85439-3.
[19] R. Chen, C. Yang, W. Cai, H.Y. Wang, J. Miao, L. Zhang, S. Chen, B. Liu, Use of platinum as the counter electrode to study the activity of nonprecious metal catalysts for the hydrogen evolution reaction, ACS Energy Lett. 2 (2017) 1070–1075, https://doi.org/10.1021/ACSENERGYLETT.7B00219.
[20] D. Li, Y. Li, B. Zhang, Y.H. Lui, S. Mooni, R. Chen, S. Hu, H. Ni, Insertion of platinum nanoparticles into MoS2 nanoflakes for enhanced hydrogen evolution reaction, Mater (2018), https://doi.org/10.3390/MA11091520, 2018, Vol. 11, Page 1520111520.
[21] M. Tavakkoli, N. Holmberg, R. Kronberg, H. Jiang, J. Sainio, E.I. Kauppinen, T. Kallio, K. Laasonen, Electrochemical activation of single-walled carbon nanotubes with pseudo-atomic-scale platinum for the hydrogen evolution reaction, ACS Catal. 7 (2017) 3121–3130, https://doi.org/10.1021/ACSCATAL.7B00199/SUPPL_FILE/CS7B00199_SI_001.PDF.
[22] L. Kim, C.G. Chung, Y.W. Sung, J.S. Chung, Dissolution and migration of platinum after long-term operation of a polymer electrolyte fuel cell under various

conditions, J. Power Sources 183 (2008) 524–532, https://doi.org/10.1016/J.JPOWSOUR.2008.05.062.
[23] S. Mitsushima, S. Kawahara, K. Ota, N. Kamiya, Consumption rate of Pt under potential cycling, J. Electrochem. Soc. 154 (2007) B153, https://doi.org/10.1149/1.2400596/XML.
[24] A. Kawano, S. Imabayashi, Influence of oxygen atmosphere on dissolution of platinum under potential cycling, J. Electrochem. Soc. 161 (2014) F67–F71, https://doi.org/10.1149/2.051401JES/XML.
[25] S. Cherevko, A.A. Topalov, A.R. Zeradjanin, G.P. Keeley, K.J.J. Mayrhofer, Temperature-dependent dissolution of polycrystalline platinum in sulfuric acid electrolyte, Electrocatalysis 5 (2014) 235–240, https://doi.org/10.1007/S12678-014-0187-0/FIGURES/3.
[26] M. Matsumoto, T. Miyazaki, H. Imai, Oxygen-enhanced dissolution of platinum in acidic electrochemical environments, J. Phys. Chem. C. 115 (2011) 11163–11169, https://doi.org/10.1021/JP201959H/ASSET/IMAGES/JP201959H.SOCIAL.JPEG_V03.
[27] G. Dong, M. Fang, H. Wang, S. Yip, H.Y. Cheung, F. Wang, C.Y. Wong, S.T. Chu, J. C. Ho, Insight into the electrochemical activation of carbon-based cathodes for hydrogen evolution reaction, J. Mater. Chem. A. 3 (2015) 13080–13086, https://doi.org/10.1039/C5TA02551F.
[28] Z. Shi, K. Nie, Z.J. Shao, B. Gao, H. Lin, H. Zhang, B. Liu, Y. Wang, Y. Zhang, X. Sun, X.M. Cao, P. Hu, Q. Gao, Y. Tang, Phosphorus-Mo 2 C@carbon nanowires toward efficient electrochemical hydrogen evolution: composition, structural and electronic regulation, Energy Environ. Sci. 10 (2017) 1262–1271, https://doi.org/10.1039/C7EE00388A.
[29] M. Tian, C. Cousins, D. Beauchemin, Y. Furuya, A. Ohma, G. Jerkiewicz, Influence of the working and counter electrode surface area ratios on the dissolution of platinum under electrochemical conditions, ACS Catal. 6 (2016) 5108–5116, https://doi.org/10.1021/ACSCATAL.6B00200/ASSET/IMAGES/ACSCATAL.6B00200.SOCIAL.JPEG_V03.
[30] R. Wei, M. Fang, G. Dong, J.C. Ho, Is platinum a suitable counter electrode material for electrochemical hydrogen evolution reaction?, (2017). https://doi.org/10.1016/j.scib.2017.06.006.
[31] G. Jerkiewicz, Applicability of platinum as a counter-electrode material in electrocatalysis research, ACS Catal. 12 (2022) 2661–2670, https://doi.org/10.1021/ACSCATAL.1C06040/ASSET/IMAGES/LARGE/CS1C06040_0004.JPEG.
[32] J. Xie, L. Gao, H. Jiang, X. Zhang, F. Lei, P. Hao, B. Tang, Y. Xie, Platinum nanocrystals decorated on defect-rich MoS2 nanosheets for pH-universal hydrogen evolution reaction, Cryst. Growth Des. 19 (2019) 60–65, https://doi.org/10.1021/ACS.CGD.8B01594/SUPPL_FILE/CG8B01594_SI_001.PDF.
[33] K. Tang, X. Wang, Q. Li, C. Yan, K. Tang, X. Wang, Q. Li, C. Yan, High edge selectivity of in situ electrochemical Pt deposition on edge-rich layered WS2 nanosheets, Adv. Mater. 30 (2018), 1704779, https://doi.org/10.1002/ADMA.201704779.
[34] H.Y. Jung, M.J. Chae, J.H. Park, Y. Il Song, J.C. Ro, S.J. Suh, Effects of platinum group metals on MoS2nanosheets for a high-performance hydrogen evolution reaction catalyst, ACS Appl. Energy Mater. 4 (2021) 10748–10755, https://doi.org/10.1021/ACSAEM.1C01721/SUPPL_FILE/AE1C01721_SI_001.PDF.
[35] J. Shao, Y. Li, M. Zhong, Q. Wang, X. Luo, K. Li, W. Zhao, Enhanced-performance flexible supercapacitor based on Pt-doped MoS2, Mater. Lett. 252 (2019) 173–177, https://doi.org/10.1016/J.MATLET.2019.05.124.
[36] X. Jian, T. Li, S. Guo, L. Gao, F. Fu, Y. Tian, Y. Wu, Platinum nanoparticle-electrodeposited Ti3C2TxMXene as a binder-free electrocatalyst for improved hydrogen evolution, ACS Appl. Energy Mater. 5 (2022) 3092–3099, https://doi.org/10.1021/ACSAEM.1C03708/SUPPL_FILE/AE1C03708_SI_001.PDF.
[37] T.Y. Ko, A. Jeong, W. Kim, J. Lee, Y. Kim, J.E. Lee, G.H. Ryu, K. Park, D. Kim, Z. Lee, M.H. Lee, C. Lee, S. Ryu, On-stack two-dimensional conversion of MoS2 into MoO3, 2D Mater. 4 (2016), 014003, https://doi.org/10.1088/2053-1583/4/1/014003.
[38] D. Lee, J. Hyuck Jang, W. Song, J. Moon, Y. Kim, J. Lee, B. Jeong, S. Park, In situ work-function measurement during chemical transformation of MoS2 to MoO3 by ambient-pressure x-ray photoelectron spectroscopy, 2D Mater. 7 (2020), 025014, https://doi.org/10.1088/2053-1583/AB6780.
[39] M. Hou, Y. Qiu, G. Yan, J. Wang, D. Zhan, X. Liu, J. Gao, L. Lai, Aging mechanism of MoS2 nanosheets confined in N-doped mesoporous carbon spheres for sodium-ion batteries, Nano Energy 62 (2019) 299–309, https://doi.org/10.1016/J.NANOEN.2019.05.048.
[40] H.S. Kim, J.B. Cook, H. Lin, J.S. Ko, S.H. Tolbert, V. Ozolins, B. Dunn, Oxygen vacancies enhance pseudocapacitive charge storage properties of MoO3-x, Nat. Mater. 16 (2017) 454–462, https://doi.org/10.1038/NMAT4810.
[41] P. Qin, S.Q. Zhang, K.K.L. Yung, Z.F. Huang, B. Gao, Disclosure of charge storage mechanisms in molybdenum oxide nanobelts with enhanced supercapacitive performance induced by oxygen deficiency, Rare Met. 40 (2021) 2447–2454, https://doi.org/10.1007/S12598-021-01722-3/FIGURES/5.
[42] X. Cai, X.G. Sang, Y. Song, D. Guo, X.X. Liu, X. Sun, Activating the highly reversible Mo4+/Mo5+ redox couple in amorphous molybdenum oxide for high-performance supercapacitors, ACS Appl. Mater. Interfaces. 12 (2020) 48565–48571, https://doi.org/10.1021/ACSAMI.0C13692.
[43] T. Sun, Z. Li, X. Liu, L. Ma, J. Wang, S. Yang, Facile construction of 3D graphene/MoS2 composites as advanced electrode materials for supercapacitors, J. Power Sources 331 (2016) 180–188, https://doi.org/10.1016/J.JPOWSOUR.2016.09.036.
[44] M.A. Bissett, I.A. Kinloch, R.A.W. Dryfe, Characterization of MoS2-graphene composites for high-performance coin cell supercapacitors, ACS Appl. Mater. Interfaces. 7 (2015) 17388–17398, https://doi.org/10.1021/ACSAMI.5B04672.
[45] H. Wang, Z. Lu, S. Xu, D. Kong, J.J. Cha, G. Zheng, P.C. Hsu, K. Yan, D. Bradshaw, F.B. Prinz, Y. Cui, Electrochemical tuning of vertically aligned MoS2 nanofilms and its application in improving hydrogen evolution reaction, Proc. Natl. Acad. Sci. U. S. A. 110 (2013) 19701–19706, https://doi.org/10.1073/PNAS.1316792110.
[46] M. Mortazavi, C. Wang, J. Deng, V.B. Shenoy, N.V. Medhekar, Ab initio characterization of layered MoS2 as anode for sodium-ion batteries, J. Power Sources. 268 (2014) 279–286, https://doi.org/10.1016/J.JPOWSOUR.2014.06.049.
[47] Z. Hu, L. Wang, K. Zhang, J. Wang, F. Cheng, Z. Tao, J. Chen, MoS2 nanoflowers with expanded interlayers as high-performance anodes for sodium-ion batteries, Angew. Chem. Int. Ed. 53 (2014) 12794–12798, https://doi.org/10.1002/ANIE.201407898.
[48] Z. Li, K. Jiang, F. Khan, A. Goswami, J. Liu, A. Passian, T. Thundat, Anomalous interfacial stress generation during sodium intercalation/extraction in MoS 2 thin-film anodes, Sci. Adv. 5 (2019), https://doi.org/10.1126/SCIADV.AAV2820/SUPPL_FILE/AAV2820_SM.PDF.
[49] M. Szkoda, K. Trzciński, K. Siuzdak, A. Lisowska-Oleksiak, Photocatalytical properties of maze-like MoO3 microstructures prepared by anodization of Mo plate, Electrochim. Acta. 228 (2017) 139–145, https://doi.org/10.1016/J.ELECTACTA.2017.01.064.
[50] M. Ranjba, F. Delalat, H. Salamati, Molybdenum oxide nanosheets prepared by an anodizing-exfoliation process and observation of photochromic properties, Appl. Surf. Sci. 396 (2017) 1752–1759, https://doi.org/10.1016/J.APSUSC.2016.11.225.
[51] F. Delalat, M. Ranjbar, H. Salamati, Blue colloidal nanoparticles of molybdenum oxide by simple anodizing method: decolorization by PdCl2 and observation of in-liquid gasochromic coloration, Sol. Energy Mater. Sol. Cells 144 (2016) 165–172, https://doi.org/10.1016/J.SOLMAT.2015.08.038.
[52] N. Dukstiene, L. Tatariskinaite, M. Andrulevicius, Characterization of electrochemically deposited thin Mo-O-C-Se film layers, Mater. Sci. 28 (2010).
[53] Y. Mao, W. Li, X. Sun, Y. Ma, J. Xia, Y. Zhao, X. Lu, J. Gan, Z. Liu, J. Chen, P. Liu, Y. Tong, Room-temperature ferromagnetism in hierarchically branched MoO 3 nanostructures, CrystEngComm. 14 (2012) 1419–1424, https://doi.org/10.1039/C1CE05700F.
[54] H. Komatsu, S. Ozuka, K. Ogura, Cathodic deposition of molybdenum and vanadium mixed oxyhydroxide films from V-substituted polymolybdophosphate, Electrochim. Acta 51 (2005) 274–280, https://doi.org/10.1016/J.ELECTACTA.2005.04.025.
[55] G.E. Buono-Core, A.H. Klahn, C. Castillo, E. Muñoz, C. Manzur, G. Cabello, B. Chornik, Synthesis and characterization of thin molybdenum oxide films prepared from molybdenum dioxo tropolonate precursors by photochemical metal-organic deposition (PMOD) and its evaluation as ammonia gas sensors, J. Non Cryst. Solids 387 (2014) 21–27, https://doi.org/10.1016/J.JNONCRYSOL.2013.12.009.
[56] J. Gong, Y. Kong, J. Li, X. Wang, Y. Que, Z. Zhang, Z. Ding, X. Xiao, Role of surface microstructure of Mo back contact on alkali atom diffusion and Ga grading in Cu(In,Ga)Se2 thin film solar cells, Energy Sci. Eng. 7 (2019) 754–763, https://doi.org/10.1002/ESE3.304.
[57] M. Szkoda, K. Trzciński, A.P. Nowak, M. Gazda, M. Sawczak, A. Lisowska-Oleksiak, The effect of morphology and crystalline structure of Mo/MoO3 layers on photocatalytic degradation of water organic pollutants, Mater. Chem. Phys. 248 (2020), 122908, https://doi.org/10.1016/J.MATCHEMPHYS.2020.122908.
[58] W. Wang, X. Zeng, J.H. Warner, Z. Guo, Y. Hu, Y. Zeng, J. Lu, W. Jin, S. Wang, J. Lu, Y. Zeng, Y. Xiao, Photoresponse-bias modulation of a high-performance MoS 2 photodetector with a unique vertically stacked 2H-MoS 2/1T@2H-MoS 2 structure, ACS Appl. Mater. Interfaces. 12 (2020) 33325–33335, https://doi.org/10.1021/ACSAMI.0C04048.
[59] M. Chen, B. Ji, Z. Dai, X. Du, B. He, G. Chen, D. Liu, S. Chen, K.H. Lo, S. Wang, B. Zhou, H. Pan, Vertically-aligned 1T/2H-MS2 (M = Mo, W) nanosheets for surface-enhanced Raman scattering with long-term stability and large-scale uniformity, Appl. Surf. Sci. 527 (2020), 146769, https://doi.org/10.1016/J.APSUSC.2020.146769.
[60] G. Eda, H. Yamaguchi, D. Voiry, T. Fujita, M. Chen, M. Chhowalla, Photoluminescence from chemically exfoliated MoS2, Nano Lett. 11 (2011) 5111–5116, https://doi.org/10.1021/NL201874W.
[61] A. Naujokaitis, P. Gaigalas, C. Bittencourt, S. Mickevičius, A. Jagminas, 1T/2H MoS2/MoO3 hybrid assembles with glycine as highly efficient and stable electrocatalyst for water splitting, Int. J. Hydrog. Energy 44 (2019) 24237–24245, https://doi.org/10.1016/J.IJHYDENE.2019.07.161.
[62] Z. Zhang, Y. Dong, G. Liu, J. Li, H. Sun, H. Luo, S. Liu, The ultrafine monolayer 1 T/2H-MoS2: preparation, characterization and amazing photocatalytic characteristics, Colloids Surf. A Physicochem. Eng. Asp. 589 (2020), 124431, https://doi.org/10.1016/J.COLSURFA.2020.124431.
[63] Y. Qi, Q. Xu, Y. Wang, B. Yan, Y. Ren, Z. Chen, CO2-Induced Phase Engineering: protocol for Enhanced Photoelectrocatalytic Performance of 2D MoS2 Nanosheets, ACS Nano 10 (2016) 2903–2909, https://doi.org/10.1021/ACSNANO.6B00001/SUPPL_FILE/NN6B00001_SI_001.PDF.
[64] C. Zhu, Q. Xian, Q. He, C. Chen, W. Zou, C. Sun, S. Wang, X. Duan, Edge-Rich Bicrystalline 1T/2H-MoS 2 cocatalyst-decorated {110} terminated CeO 2 nanorods for photocatalytic hydrogen evolution, ACS Appl. Mater. Interfaces 13 (2021) 35818–35827, https://doi.org/10.1021/ACSAMI.1C09651.
[65] M. Wu, J. Zhan, K. Wu, Z. Li, L. Wang, B. Geng, L. Wang, D. Pan, Metallic 1T MoS 2 nanosheet arrays vertically grown on activated carbon fiber cloth for enhanced Li-ion storage performance, J. Mater. Chem. A. 5 (2017) 14061–14069, https://doi.org/10.1039/C7TA03497K.

[66] X. Lin, D. Xue, L. Zhao, F. Zong, X. Duan, X. Pan, J. Zhang, Q. Li, In-situ growth of 1T/2H-MoS2 on carbon fiber cloth and the modification of SnS2 nanoparticles: a three-dimensional heterostructure for high-performance flexible lithium-ion batteries, Chem. Eng. J. 356 (2019) 483–491, https://doi.org/10.1016/J.CEJ.2018.08.208.

[67] L. Kumari, Y.R. Ma, C.C. Tsai, Y.W. Lin, S.Y. Wu, K.W. Cheng, Y. Liou, X-ray diffraction and Raman scattering studies on large-area array and nanobranched structure of1D MoO2 nanorods, Nanotechnology 18 (2007), 115717, https://doi.org/10.1088/0957-4484/18/11/115717.

[68] S. Alizadeh, S.A. Hassanzadeh-Tabrizi, MoO3 fibers and belts: molten salt synthesis, characterization and optical properties, Ceram. Int. 41 (2015) 10839–10843, https://doi.org/10.1016/J.CERAMINT.2015.05.024.

[69] K. Momma, F. Izumi, VESTA3 for three-dimensional visualization of crystal, volumetric and morphology data, Urn:Issn:0021-8898. 44 (2011) 1272–1276. https://doi.org/10.1107/S0021889811038970.

[70] X. Guan, Y. Ren, S. Chen, J. Yan, G. Wang, H. Zhao, W. Zhao, Z. Zhang, Z. Deng, Y. Zhang, Y. Dai, L. Zou, R. Chen, C. Liu, Charge separation and strong adsorption-enhanced MoO3 visible light photocatalytic performance, J. Mater. Sci. 55 (2020) 5808–5822, https://doi.org/10.1007/S10853-020-04418-8/FIGURES/12.

[71] H. Hu, C. Deng, J. Xu, K. Zhang, M. Sun, Metastable h-MoO3 and stable α-MoO3 microstructures: controllable synthesis, growth mechanism and their enhanced photocatalytic activity, 10 (2015) 1336–1346. https://doi.org/10.1080/17458080.2015.1012654.

[72] X. Zhang, X. Zeng, M. Yang, Y. Qi, Investigation of a branchlike MoO3/polypyrrole hybrid with enhanced electrochemical performance used as an electrode in supercapacitors, ACS Appl. Mater. Interfaces. 6 (2014) 1125–1130, https://doi.org/10.1021/AM404724U/ASSET/IMAGES/AM404724U.SOCIAL.JPEG_V03.

[73] J.S. Kang, J. Kim, M.J. Lee, Y.J. Son, D.Y. Chung, S. Park, J. Jeong, J.M. Yoo, H. Shin, H. Choe, H.S. Park, Y.E. Sung, Electrochemically synthesized nanoporous molybdenum carbide as a durable electrocatalyst for hydrogen evolution reaction, Adv. Sci. 5 (2018), 1700601, https://doi.org/10.1002/ADVS.201700601.

[74] A.L. Tan, S.S. Ng, H.A. Hassan, Influence of initial sulfur content in precursor solution for the growth of molybdenum disulfide, J. Phys. Conf. Ser. 995 (2018), 012060, https://doi.org/10.1088/1742-6596/995/1/012060.

[75] K. Shomalian, M.M. Bagheri-Mohagheghi, M. Ardyanian, Synthesis and characterization of porous nanoparticles of molybdenum sulfide (MoS2) chalcogenide semiconductor prepared by polymerizing-complexing sol–gel method, J. Mater. Sci. Mater. Electron. 28 (2017) 14331–14340, https://doi.org/10.1007/S10854-017-7293-8/FIGURES/10.

[76] Y. Wang, M. Zhen, H. Liu, C. Wang, Interlayer-expanded MoS2/graphene composites as anode materials for high-performance lithium-ion batteries, J. Solid State Electrochem. 22 (2018) 3069–3076, https://doi.org/10.1007/S10008-018-4018-8/FIGURES/6.

[77] X. Zeng, L. Niu, L. Song, X. Wang, X. Shi, J. Yan, Effect of polymer addition on the structure and hydrogen evolution reaction property of nanoflower-like molybdenum disulfide, Met 5 (2015) 1829–1844, https://doi.org/10.3390/MET5041829, 2015, Vol. 5, Pages 1829-1844.

[78] H. Liu, X. Chen, L. Deng, M. Ding, J. Li, X. He, Perpendicular growth of few-layered MoS 2 nanosheets on MoO 3 nanowires fabricated by direct anion exchange reactions for high-performance lithium-ion batteries, J. Mater. Chem. A 4 (2016) 17764–17772, https://doi.org/10.1039/C6TA06741G.

[79] Y. Dong, X. Xu, S. Li, C. Han, K. Zhao, L. Zhang, C. Niu, Z. Huang, L. Mai, Inhibiting effect of Na+ pre-intercalation in MoO3 nanobelts with enhanced electrochemical performance, Nano Energy 15 (2015) 145–152, https://doi.org/10.1016/J.NANOEN.2015.04.015.

[80] F. Cheng, Z. Tao, J. Chen, Vapor-transportation preparation and reversible lithium intercalation/deintercalation of α-MoO3 microrods, J. Phys. Chem. B 110 (2005) 119–124, https://doi.org/10.1021/JP0553784.

[81] X.J. Wang, R. Nesper, C. Villevieille, P. Novák, Ammonolyzed MoO3 Nanobelts as Novel Cathode Material of Rechargeable Li-Ion Batteries, Adv. Energy Mater. 3 (2013) 606–614, https://doi.org/10.1002/AENM.201200692.

[82] P. Thangasamy, N. Ilayaraja, D. Jeyakumar, M. Sathish, Electrochemical cycling and beyond: unrevealed activation of MoO3 for electrochemical hydrogen evolution reactions, Chem. Commun. 53 (2017) 2245–2248, https://doi.org/10.1039/C6CC09187C.

[83] H. Wei, X. Yan, S. Wu, Z. Luo, S. Wei, Z. Guo, Electropolymerized Polyaniline Stabilized Tungsten Oxide Nanocomposite Films: electrochromic Behavior and Electrochemical Energy Storage, J. Phys. Chem. C. 116 (2012) 25052–25064, https://doi.org/10.1021/JP3090777.

[84] M. Nawwar, R. Poon, R. Chen, R.P. Sahu, I.K. Puri, I. Zhitomirsky, High areal capacitance of Fe3O4-decorated carbon nanotubes for supercapacitor electrodes, Carbon Energy 1 (2019) 124–133, https://doi.org/10.1002/CEY2.6.

[85] R. Yuksel, C. Durucan, H.E. Unalan, Ternary nanocomposite SWNT/WO3/PANI thin film electrodes for supercapacitors, J. Alloy. Compd. 658 (2016) 183–189, https://doi.org/10.1016/J.JALLCOM.2015.10.216.

[86] B.A. Mei, O. Munteshari, J. Lau, B. Dunn, L. Pilon, Physical Interpretations of Nyquist Plots for EDLC Electrodes and Devices, J. Phys. Chem. C. 122 (2018) 194–206, https://doi.org/10.1021/ACS.JPCC.7B10582/SUPPL_FILE/JP7B10582_SI_001.ZIP.

[87] V. Sunil, B. Pal, I. Izwan Misnon, R. Jose, Characterization of supercapacitive charge storage device using electrochemical impedance spectroscopy, Mater. Today Proc. 46 (2021) 1588–1594, https://doi.org/10.1016/J.MATPR.2020.07.248.

[88] R. Tatara, P. Karayaylali, Y. Yu, Y. Zhang, L. Giordano, F. Maglia, R. Jung, J. P. Schmidt, I. Lund, Y. Shao-Horn, The Effect of Electrode-Electrolyte Interface on the Electrochemical Impedance Spectra for Positive Electrode in Li-Ion Battery, J. Electrochem. Soc. 166 (2019) A5090–A5098, https://doi.org/10.1149/2.0121903JES/XML.

[89] Z.M. Marković, M.D. Budimir, D.P. Kepić, I.D. Holclajtner-Antunović, M. T. Marinović-Cincović, M.D. Dramićanin, V.D. Spasojević, D.B. Peruško, Z. Špitalský, M. Mičušik, V.B. Pavlović, B.M. Todorović-Marković, Semi-transparent, conductive thin films of electrochemical exfoliated graphene, RSC Adv. 6 (2016) 39275–39283, https://doi.org/10.1039/C6RA04250C.

[90] S. García-Dalí, J.I. Paredes, J.M. Munuera, S. Villar-Rodil, A. Adawy, A. Martínez-Alonso, J.M.D. Tascón, Aqueous Cathodic Exfoliation Strategy toward Solution-Processable and Phase-Preserved MoS2 Nanosheets for Energy Storage and Catalytic Applications, ACS Appl. Mater. Interfaces. 11 (2019) 36991–37003, https://doi.org/10.1021/ACSAMI.9B13484/SUPPL_FILE/AM9B13484_SI_001.PDF.

[91] N. Liu, P. Kim, J.H. Kim, J.H. Ye, S. Kim, C.J. Lee, Large-Area Atomically Thin MoS2 Nanosheets Prepared Using Electrochemical Exfoliation, ACS Nano 8 (2014) 6902–6910, https://doi.org/10.1021/NN5016242.

[92] X. You, N. Liu, C.J. Lee, J.J. Pak, An electrochemical route to MoS2 nanosheets for device applications, Mater. Lett. 121 (2014) 31–35, https://doi.org/10.1016/J.MATLET.2014.01.052.

[93] S.A. Ansari, H. Fouad, S.G. Ansari, M.P. Sk, M.H. Cho, Mechanically exfoliated MoS2 sheet coupled with conductive polyaniline as a superior supercapacitor electrode material, J. Colloid Interface Sci. 504 (2017) 276–282, https://doi.org/10.1016/J.JCIS.2017.05.064.

[94] R.B. Choudhary, M. Majumder, A.K. Thakur, Two-Dimensional Exfoliated MoS2 Flakes Integrated with Polyindole for Supercapacitor Application, ChemistrySelect 4 (2019) 6906–6912, https://doi.org/10.1002/SLCT.201901558.

[95] P. Karthika, N. Rajalakshmi, K.S. Dhathathreyan, Functionalized exfoliated graphene oxide as supercapacitor electrodes, Soft Nanosci. Lett. 2012 (2012) 59–66, https://doi.org/10.4236/SNL.2012.24011.

[96] S. Mukherjee, J. Turnley, E. Mansfield, J. Holm, D. Soares, L. David, G. Singh, Exfoliated transition metal dichalcogenide nanosheets for supercapacitor and sodium ion battery applications, R. Soc. Open Sci. 6 (2019), https://doi.org/10.1098/RSOS.190437.

[97] L. Jiang, S. Zhang, S.A. Kulinich, X. Song, J. Zhu, X. Wang, H. Zeng, Optimizing hybridization of 1T and 2H phases in MoS2 monolayers to improve capacitances of supercapacitors, Mater. Res. Lett. 3 (2015) 177–183, https://doi.org/10.1080/21663831.2015.1057654/SUPPL_FILE/TMRL_A_1057654_SM6377.DOC.

[98] L. Xing, M.A. Hossain, M. Tian, D. Beauchemin, K.T. Adjemian, G. Jerkiewicz, Platinum electro-dissolution in acidic media upon potential cycling, Electrocatalysis 5 (2014) 96–112, https://doi.org/10.1007/S12678-013-0167-9/FIGURES/11.

[99] A.A. Topalov, I. Katsounaros, M. Auinger, S. Cherevko, J.C. Meier, S.O. Klemm, K. J.J. Mayrhofer, Dissolution of Platinum: limits for the Deployment of Electrochemical Energy Conversion? Angew. Chemie Int. Ed. 51 (2012) 12613–12615, https://doi.org/10.1002/ANIE.201207256.

[100] Y. Sugawara, T. Okayasu, A.P. Yadav, A. Nishikata, T. Tsuru, Dissolution mechanism of platinum in sulfuric acid solution, J. Electrochem. Soc. 159 (2012) F779–F786, https://doi.org/10.1149/2.017212JES/XML.

[101] H. Imai, K. Izumi, M. Matsumoto, Y. Kubo, K. Kato, Y. Imai, In situ and real-time monitoring of oxide growth in a few monolayers at surfaces of platinum nanoparticles in aqueous media, J. Am. Chem. Soc. 131 (2009) 6293–6300, https://doi.org/10.1021/JA810036H/SUPPL_FILE/JA810036H_SI_001.PDF.

[102] X. Cai, Y. Song, S.Q. Wang, X. Sun, X.X. Liu, Extending the cycle life of high mass loading MoOx electrode for supercapacitor applications, Electrochim. Acta. 325 (2019), 134877, https://doi.org/10.1016/J.ELECTACTA.2019.134877.

[103] M.T. Greiner, L. Chai, M.G. Helander, W.M. Tang, Z.H. Lu, Metal/Metal-Oxide Interfaces: how Metal Contacts Affect the Work Function and Band Structure of MoO3, Adv. Funct. Mater. 23 (2013) 215–226, https://doi.org/10.1002/ADFM.201200993.

[104] M.T. Greiner, L. Chai, M.G. Helander, W.M. Tang, Z.H. Lu, Transition Metal Oxide Work Functions: the Influence of Cation Oxidation State and Oxygen Vacancies, Adv. Funct. Mater. 22 (2012) 4557–4568, https://doi.org/10.1002/ADFM.201200615.

[105] L. Huang, B. Yao, J. Sun, X. Gao, J. Wu, J. Wan, T. Li, Z. Hu, J. Zhou, Highly conductive and flexible molybdenum oxide nanopaper for high volumetric supercapacitor electrode, J. Mater. Chem. A. 5 (2017) 2897–2903, https://doi.org/10.1039/C6TA10433A.

[106] P. Guha, B. Mohanty, R. Thapa, R.M. Kadam, P.V. Satyam, B.K. Jena, Defect-Engineered MoO2Nanostructures as an Efficient Electrocatalyst for Oxygen Evolution Reaction, ACS Appl. Energy Mater. 3 (2020) 5208–5218, https://doi.org/10.1021/ACSAEM.9B02551/SUPPL_FILE/AE9B02551_SI_001.PDF.

[107] al - K.-Y. Huang, Y.-.H. Luo, H.-.M. Cheng, S. Mohammadi, M. Ali Taher, H. Beitollahi, P. Guha, A. Ghosh, A. Sarkar, S. Mandal, S.K. Ray, D.K. Goswami, P. V. Satyam, P-type β-MoO2 nanostructures on n-Si by hydrogenation process: synthesis and application towards self-biased UV-visible photodetection, Nanotechnology 30 (2018), 035204, https://doi.org/10.1088/1361-6528/AAEADC.

[108] L. Brewer, R.H. Lamoreaux, The Mo-O system (Molybdenum-Oxygen), Bull. Alloy Phase Diagrams 1 (1980) 85–89, https://doi.org/10.1007/BF02881199, 1980 12.

[109] T.-.C. Liu, W.G. Pell, B.E. Conway, S.L. Roberson, Behavior of Molybdenum Nitrides as Materials for Electrochemical Capacitors: comparison with Ruthenium

Oxide, J. Electrochem. Soc. 145 (1998) 1882–1888, https://doi.org/10.1149/1.1838571/XML.
[110] P. Simon, Y. Gogotsi, B. Dunn, Where do batteries end and supercapacitors begin? Science 343 (2014) 1210–1211, https://doi.org/10.1126/science.1249625 (80-.).
[111] K. Brezesinski, J. Wang, J. Haetge, C. Reitz, S.O. Steinmueller, S.H. Tolbert, B. M. Smarsly, B. Dunn, T. Brezesinski, Pseudocapacitive Contributions to Charge Storage in Highly Ordered Mesoporous Group V Transition Metal Oxides with Iso-Oriented Layered Nanocrystalline Domains, J. Am. Chem. Soc. 132 (2010) 6982–6990, https://doi.org/10.1021/JA9106385.
[112] V. Augustyn, P. Simon, B. Dunn, Pseudocapacitive oxide materials for high-rate electrochemical energy storage, Energy Environ. Sci. 7 (2014) 1597–1614, https://doi.org/10.1039/C3EE44164D.
[113] S. Ardizzone, G. Fregonara, S. Trasatti, Inner" and "outer" active surface of RuO2 electrodes, Electrochim. Acta. 35 (1990) 263–267, https://doi.org/10.1016/0013-4686(90)85068-X.
[114] Y. Tian, X. Song, J. Liu, L. Zhao, P. Zhang, L. Gao, Y. Tian, X.F. Song, J. Liu, L. Zhao, P. Zhang, L. Gao, Generation of Monolayer MoS2 with 1T Phase by Spatial-Confinement-Induced Ultrathin PPy Anchoring for High-Performance Supercapacitor, Adv. Mater. Interfaces. 6 (2019), 1900162, https://doi.org/10.1002/ADMI.201900162.
[115] H. Ji, C. Liu, T. Wang, J. Chen, Z. Mao, J. Zhao, W. Hou, G. Yang, Porous Hybrid Composites of Few-Layer MoS2 Nanosheets Embedded in a Carbon Matrix with an Excellent Supercapacitor Electrode Performance, Small 11 (2015) 6480–6490, https://doi.org/10.1002/SMLL.201502355.
[116] S. Fleischmann, J.B. Mitchell, R. Wang, C. Zhan, D.E. Jiang, V. Presser, V. Augustyn, Pseudocapacitance: from Fundamental Understanding to High Power Energy Storage Materials, Chem. Rev. 120 (2020) 6738–6782, https://doi.org/10.1021/ACS.CHEMREV.0C00170/ASSET/IMAGES/ACS.CHEMREV.0C00170.SOCIAL.JPEG_V03.
[117] B. Zhang, X. Ji, K. Xu, C. Chen, X. Xiong, J. Xiong, Y. Yao, L. Miao, J. Jiang, Unraveling the different charge storage mechanism in T and H phases of MoS2, Electrochim. Acta. 217 (2016) 1–8, https://doi.org/10.1016/J.ELECTACTA.2016.09.059.
[118] B. Saravanakumar, R. Shobana, G. Ravi, V. Ganesh, R. Yuvakkumar, Preparation and electrochemical characterization of Mo9O26 nanopowders for supercapacitors applications, Nano-Structures Nano-Objects 19 (2019), 100340, https://doi.org/10.1016/J.NANOSO.2019.100340.
[119] J.P. Jegal, H.K. Kim, J.S. Kim, K.B. Kim, One-pot synthesis of mixed-valence MoO x on carbon nanotube as an anode material for lithium ion batteries, J. Electroceram. 31 (2013) 218–223, https://doi.org/10.1007/S10832-013-9821-0/FIGURES/5.